Multipath Assisted Positioning with Simultaneous Localization and Mapping

Christian Gentner, *Member, IEEE,* Thomas Jost, *Member, IEEE,* Wei Wang, *Member, IEEE,* Siwei Zhang, *Member, IEEE,* Armin Dammann , *Member, IEEE,* and Uwe-Carsten Fiebig *Member, IEEE*

***Abstract*—This paper describes an algorithm that exploits multipath propagation for position estimation of mobile receivers. We apply a novel algorithm based on recursive Bayesian filtering, named Channel-SLAM. This approach treats multipath components as signals emitted from virtual transmitters which are time synchronized to the physical transmitter and static in their positions. Contrarily to other approaches, Channel-SLAM considers also paths occurring due to multiple numbers of reflections or scattering as well as the combination. Hence, each received multipath component increases the number of transmitters resulting in a more accurate position estimate or enabling positioning when the number of physical transmitters is insufficient. Channel-SLAM estimates the receiver position and the positions of the virtual transmitters simultaneously, hence, the approach does not require any prior information such as a room-layout or a database for fingerprinting. The only prior knowledge needed is the physical transmitter position as well as the initial receiver position and moving direction. Based on simulations, the position precision of Channel-SLAM is evaluated by a comparison to simplified algorithms and to the posterior Cramér-Rao lower bound. Furthermore, the paper shows the performance of Channel-SLAM based on measurements in an indoor scenario with only a single physical transmitter.**

***Index Terms*—Channel-SLAM, CRLB, multipath, positioning, particle filter, SLAM**

I. Introduction

Global navigation satellite systems (GNSSs) are the most common systems used for positioning in the world. In critical environments, such as urban canyons or indoors, the position accuracy using GNSSs might be drastically reduced. In these environments, multipath effects, low received signal power and non-line-of-sight (NLoS) propagation reduce the position accuracy [1]. To enhance the positioning performance in these scenarios, signals of opportunity (SoO) can be used for example from mobile communication base-stations [2], [3], wireless local area network (WLAN) transmitters [4] or dedicated ultra-wideband (UWB) transmitters [5]–[7]. However, still multipath propagation might reduce the accuracy. In multipath environments, the signal reaches the receive antenna by multiple paths. The range estimate of standard algorithms like the delay locked loop (DLL) is biased in multipath propagation environments [8]. Algorithms like [9]–[11] reduce the multipath error by modifying the DLL. Other approaches, estimate the channel impulse response (CIR) to mitigate multipath effects on the range estimate. Examples for these approaches are based on maximum likelihood like [12]–[14] or on recursive Bayesian filters like [15], [16].

Exploiting multipath propagation instead of mitigating the multipath effect is attracting significant research interest. For example the authors of [17], [18] use multipath propagation for positioning of a mobile terminal with a multipath fingerprinting approach. Other ideas, like [19]–[23] interpret the effect of an electromagnetic wave reflected on a surface as a signal emitted from virtual transmitters (VTs). In the field of indoor positioning with UWB signals, the approaches [21]–[23] use reflected signals with the constraints of knowing the positions of walls and of the physical transmitter. These constraints allow to precalculate the position of the VTs and hence, the estimation of the receiver position. The authors of [24] use a non-linear least square algorithm combining UWB measurements at several receiver positions to estimate the positions of the VTs and the receiver simultaneously within small scale scenarios. Furthermore, the authors of [25] estimate and track the phase information of multipath components (MPCs) using an extended Kalman filter (EKF) and estimate the user position using a time difference of arrival (TDOA) positioning approach. Additional to positioning applications, multipath propagation can be used to estimate the surrounding area, e.g., [26] uses a non-static UWB radar to estimate the room-geometry. This approach was extended in [27], where the UWB radar transceiver position is estimated in addition by using a simultaneous localization and mapping (SLAM) approach [28]–[30]. Similarly, [31] describes a SLAM approach to estimate the room-geometry as well as the receiver position based on UWB by using single time reflected MPCs.

In this paper, we propose an approach for multipath assisted positioning using wideband signals, named Channel-SLAM. Channel-SLAM enables accurate positioning even if only one physical transmitter is available. Contrarily to similar approaches [20]–[23], Channel-SLAM does not require any prior knowledge on the building layout. In order to use Channel-SLAM, the following conditions have to be met: a static environment, the presence of MPCs, a moving receiver, the knowledge of the physical transmitter position as well as an initial prior knowledge of the receiver position and moving direction to define the coordinate system. In order to estimate and track the CIRs at the receiver side, we assume that the receiver is equipped with a linear antenna

This work was supported by the DLR internal project Dependable Navigation, the European Union‘s FP7 project under grant agreement No. 287242 *E-HIMALAYA (extended-HIgh performance MAss market GNSS receiver muLti stAndard readY for mArket)* and the European Union‘s Horizon 2020 research and innovation programme under grant agreement No. 636537 *HIGHTS (High precision positioning for Cooperative-ITS applications)*.

C. Gentner, T. Jost, W. Wang, S. Zhang, A. Dammann and U.-C. Fiebig are with the Institute of Communications and Navigation of German Aerospace Center (DLR), Oberpfaffenhofen, 82234 Wessling.

array and the transmitter emits continuously known wideband signals. Hence, the novelty of the algorithm is to estimate the position of the receiver and the VTs simultaneously, which can be interpreted as SLAM with radio signals, see [28]–[30]. Usually, SLAM approaches estimate the user position and build a map of the environment simultaneously. Instead of mapping the environment, Channel-SLAM maps the VT positions and interprets them as landmarks. Furthermore, compared to [19]–[24], [26], [27], [31], Channel-SLAM considers also paths occurring due to multiple number of reflections or scattering as well as the combination of both effects. We demonstrate that each MPC can be treated as being emitted from a VT with unknown but fixed position. Additionally, we consider positioning using wideband instead of UWB signals. UWB signals have to be of low power to be harmless to other systems which limits the coverage distance. In result, wideband signals can be used for larger distances. However, the estimation of the CIR is more challenging with wideband signals than with UWB signals [13], [14], [32]. In [33], [34], we showed that positioning is possible in NLoS scenarios using MPCs without the knowledge of the room-geometry by using Channel-SLAM and multiple transmitters. We investigated TDOA positioning and especially TDOA between MPCs where synchronization between physical transmitters is not essential. We extended [33], [34], by using a gyroscope to obtain heading information of the moving receiver and showed that positioning with only one physical transmitter is possible if MPCs and a gyroscope are used, see [35], [36]. In this contribution, we derive a novel algorithm based on Rao-Blackwellization [37]. The derived algorithm reduces the computational complexity compared to [33]–[36] and allows to use different numbers of particles in each particle filter (PF) associated to a VT. Based on simulations, we compare the accuracy of Channel-SLAM to a derived posterior Cramér-Rao lower bound (PCRLB) and to four simplified algorithms. In the considered scenario, the line-of-sight (LoS) path is received only for the first half of the simulated receiver trajectory. These artificial simulations show by a simplified scenario that even when the LoS path is not present anymore, Channel-SLAM is able to estimate the receiver position using MPCs. Positioning algorithms like [16] interpret the first arrived path as the LoS path and calculate biased position estimates. Additionally, we show the performance of Channel-SLAM with channel sounder measurement data captured in an indoor scenario which considers similarly to the simulated scenario a partially NLoS situation. Here, the receiver is turning from a corridor where the transmitter is located into another room where the LoS path between transmitter and receiver is blocked. Equivalently to the simulations, the measurement evaluations show that positioning is possible if MPCs are used.

The paper is structured as follows: Section II addresses the signal model. Thereafter, in Section III we derive the proposed algorithm, where we describe in Section III-A Channel-SLAM using a recursive Bayesian filtering approach, in Section III-B the Rao-Blackwellized particle filter (RBPF) and in Section III-C the implementation. Afterwards, we derive in Section IV the PCRLB for Channel-SLAM. In Section V-A, we evaluate the proposed algorithm and compare the result to the PCRLB and to four simplified algorithms. Thereafter, in Section V-B we show the performance of Channel-SLAM based on measurements in an indoor environment, using only one physical transmitter. Section VI briefly discusses potential applications and resulting issues of the proposed tracking algorithm. Finally, Section VII concludes the paper.

Throughout the paper, we will use the following notations:

- $(\cdot)^T$ and $(\cdot)^H$ stand for matrix (or vector) transpose and conjugate transpose, respectively.
- All vectors are interpreted as column vectors.
- $\mathbf{I}$ denotes an identity matrix.
- Matrices are denoted by bold capital letters and vectors by bold small letters.
- $[\mathbf{A}]_{l,m}$ represents the element in row l and column m of matrix $\mathbf{A}$ and $[\mathbf{x}]_l$ denotes the l-th element of vector $\mathbf{x}$.
- $\|\mathbf{A}\|^2 = \sum_l \sum_m |[\mathbf{A}]_{l,m}|^2$ represents the square of the Frobenius norm of $\mathbf{A}$.
- $a \sim \mathcal{N}\left(\mu_a, \sigma_a^2\right)$ denotes a Gaussian distributed random variable a with mean μ_a and variance σ_a^2.
- $\mathbf{E}[x]$ stands for expectation or sample mean of x.
- $1:k$ stands for all integer numbers starting from 1 to k, thus $1, 2, \ldots, k$.
- $\Re\{x\}$ denotes the real part of x.
- c is the speed of light.
- $\hat{x}$ denotes the estimation of x.
- $\propto$ stands for proportional.
- $\{x^{(i)}\}_{i=1}^N$ defines the set for x_i with $i = 1, \ldots, N$.

II. Formulation of the Signal Model

In wireless propagation the transmitted signal is reflected and scattered by objects. Thus, the transmitted signal $s(t)$ reaches the receive antenna via multiple geometric paths. According to [38], the CIR $h(t,\tau)$ at time t can be assumed to be constant for a short time interval T, with

$$h(t,\tau) = \sum_{i=0}^{N(t)-1} \alpha_i(t) \cdot \delta\left(\tau - \tau_i(t)\right) , \tag{1}$$

for $T_0 \leq t_k \leq T_0 + T$, where $N(t)$ is the number of paths, $\alpha_i(t)$ the complex amplitude, $\tau_i(t)$ the delay of the i-th path for $i = 0, \ldots, N(t)-1$ and $\delta(\tau)$ stands for the Dirac distribution. Assuming that the transmitted signal $s(t)$ is time limited with a length smaller than T, the signal received by the l-th antenna at time t_k sampled with rate B, bin indices $m = 0, \ldots, M-1$ and the delay $\tau_m = \frac{m}{B}$ can be written as

$$\begin{aligned} y_l(t_k,\tau_m) &= \sum_{i=0}^{N(t_k)-1} \alpha_i(t_k)\, b_l(\phi_i(t_k))\, s(\tau_m - \tau_i(t_k)) + n(\tau_m) \\ &= \tilde{y}_l(t_k,\tau_m) + n(\tau_m) , \end{aligned} \tag{2}$$

for $T_0 \leq t_k \leq T_0 + T$, where $b_l(\phi_i(t_k))$ denotes the response of the l-th receive antenna with respect to the phase center, $\phi_i(t_k)$ the angle of arrival (AoA)[1], $\tilde{y}_l(t_k,\tau_m)$ is the sum of all paths' contributions and $n(\tau_m)$ denotes white circular

[1]Please note, that the expression given in (2) considers a linear antenna array only. An extension to other types of antenna arrays able to measure the two dimensional AoA separately is straightforward.

symmetric normal distributed receiver noise with variance σ_n^2. Using matrix notation, $\tilde{\mathbf{Y}}(t_k) = [\tilde{\mathbf{y}}(t_k, \tau_0), \ldots, \tilde{\mathbf{y}}(t_k, \tau_{M-1})]$ denotes the sum of all paths' contribution for all antennas $l = 1, \ldots, L$ with $\tilde{\mathbf{y}}(t_k, \tau_m) = [\tilde{y}_1(t_k, \tau_m), \ldots, \tilde{y}_L(t_k, \tau_m)]^T$ and respectively the sampled received signal $\boldsymbol{Y}(t_k) = [\boldsymbol{y}(t_k, \tau_0), \ldots, \boldsymbol{y}(t_k, \tau_{M-1})]$ with $\boldsymbol{y}(t_k, \tau_m) = [y_1(t_k, \tau_m), \ldots, y_L(t_k, \tau_m)]^T$. For a transmitter which emits the signal $s(t)$ periodically with period T_p, the receiver may measure $\boldsymbol{Y}(t_k)$ for $k = 0, \ldots, \infty$ with $t_{k+1} - t_k = T_p < T$.

In order to use MPCs to localize the receiver, a model reflecting their parameters in dependency of the user position $\boldsymbol{r}_u(t_k)$ needs to be found. In the following, we consider a static environment with a physical transmitter at position $\boldsymbol{r}_t$ and a receiver moving along an arbitrary trajectory. We consider two propagation effects in this paper: reflection and scattering. For reflection, we consider the effect of an electromagnetic wave reflected by a large smooth surface. The propagation effect of scattering occurs if an electromagnetic wave impinges an object and the energy is spread out in all directions [39]. Geometrically, the effect of scattering can be described as a fixed point S at position $\boldsymbol{r}_s$ in the pathway of the MPC.

Fig. 1 summarizes three different propagation cases, a detailed description can be found in [33]–[36]. First, we consider the case of reflection on a smooth surface. The reflection point at position $\boldsymbol{r}_r(t_k)$ is moving on the surface when the receiver is in motion. As indicated in Fig. 1 by VT_1, we can construct a VT at position $\boldsymbol{r}_{\mathrm{VT},1}$ by mirroring the physical transmitter position at the reflecting surface. The distance between VT_1 and the receiver equals $d_{\mathrm{TR}}(t_k) + d_{\mathrm{RU}_1}(t_k) = \|\boldsymbol{r}_t - \boldsymbol{r}_r(t_k)\| + \|\boldsymbol{r}_r(t_k) - \boldsymbol{r}_u(t_k)\| = \|\boldsymbol{r}_{\mathrm{VT},1} - \boldsymbol{r}_u(t_k)\|$, which is the geometrical length of the reflected path, i.e. the delay of the MPC multiplied by the speed of light, where $d_{\mathrm{TR}}(t_k)$ is the distance between the transmitter and the reflection point and $d_{\mathrm{RU}_1}(t_k)$ the distance between the reflection point and the receiver. From the receiver side, both, the reflected and the virtual propagation path starting at VT_1 have the same AoA and delay. Therefore, the reflected path can be described as a direct path between VT_1 and the receiver. Using the same approach, a VT can be constructed for paths that are reflected multiple times, see also [33]–[36].

Fig. 1 provides also a visualization of scattering of the signal at the physical scatterer S. The geometrical propagation length of the scattered propagation path is equal to a direct path between a VT positioned at S and the receiver as visualized by VT_2 at position $\boldsymbol{r}_s = \boldsymbol{r}_{\mathrm{VT},2}$ in Fig. 1 with distance $d_{\mathrm{SU}}(t_k)$ plus the propagation distance $d_{\mathrm{TS}}(t_k)$ between the physical transmitter and S. Hence, the propagation length of the scattered path is $d_{\mathrm{TS}}(t_k) + d_{\mathrm{SU}}(t_k) = \|\boldsymbol{r}_t - \boldsymbol{r}_s\| + \|\boldsymbol{r}_s - \boldsymbol{r}_u(t_k)\| = \|\boldsymbol{r}_{\mathrm{VT},2} - \boldsymbol{r}_u(t_k)\| + d_{\mathrm{VT}}$ where $d_{\mathrm{TS}}(t_k) = d_{\mathrm{VT}} > 0$ is constant for all receiver positions $\boldsymbol{r}_u(t_k)$. As indicated in Fig. 1 by the winded line, additional interactions between the physical transmitter and S may occur. This holds also for cases where the transmitted signal is subject to multiple scattering occurrences.

Fig. 1 shows as well a combination of the considered multipath effects. The emitted signal from the transmitter is first scattered at S and then reflected before it reaches the receiver. When the receiver is moving, the reflection point at position $\boldsymbol{r}_{sr}(t_k)$ in Fig. 1 is moving on the surface. Hence, the VT is defined by mirroring the scatterer S at the surface as indicated by VT_3 at position $\boldsymbol{r}_{\mathrm{VT},3}$. The propagation distance is therefore $d_{\mathrm{TS}}(t_k) + d_{\mathrm{SR}}(t_k) + d_{\mathrm{RU}_2}(t_k) = d_{\mathrm{VT}} + \|\boldsymbol{r}_s - \boldsymbol{r}_{sr}(t_k)\| + \|\boldsymbol{r}_{sr}(t_k) - \boldsymbol{r}_u(t_k)\| = d_{\mathrm{VT}} + \|\boldsymbol{r}_{\mathrm{VT},3} - \boldsymbol{r}_u(t_k)\|$, where $d_{\mathrm{TS}}(t_k) = d_{\mathrm{VT}} > 0$, $d_{\mathrm{SR}}(t_k)$ is the distance between S and $\boldsymbol{r}_{sr}(t_k)$, and $d_{\mathrm{RU}_2}(t_k)$ is the distance between $\boldsymbol{r}_{sr}(t_k)$ and the receiver. As mentioned before, additional interactions between the physical transmitter and S may occur, as indicated in Fig. 1 by the winded line.

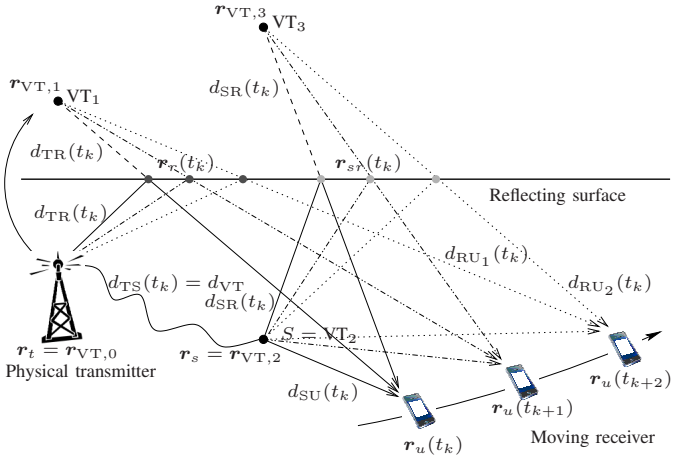

Fig. 1. The figure shows three propagation mechanism: First scenario: the transmitted signal is reflected on a smooth surface. VT_1 is defined by mirroring the physical transmitter position at the surface. Second scenario: the transmitted signal is scattered at S. VT_2 is defined at the position of S. Third scenario: The transmitted signal is scattered and afterwards reflected on a smooth surface. VT_3 is defined by mirroring the scatterer S at the surface. In the second and third scenario the additional propagation length d_{VT} equals to $d_{\mathrm{TS}}(t_k)$. Additional interactions between the physical transmitter and S may occur indicated by the winded line.

Combining the approaches described above leads to the conclusion, that the propagation path of the MPC can be equivalently described as a direct path between a VT and the receiver plus an additional constant propagation length d_{VT}. This additional propagation length is zero, i.e. $d_{\mathrm{VT}} = 0$, if only reflections occurred on the pathway between physical transmitter and receiver or greater than zero, i.e. $d_{\mathrm{VT}} > 0$, if the MPC was interacting with a scatterer. In general, d_{VT} can be interpreted as a clock offset between the VT and the physical transmitter. In the following, we will denote the position of the VT and the additional propagation length associated to the i-th MPC at time instant t_k by $\boldsymbol{r}_{\mathrm{VT},i}(t_k)$ and $d_{\mathrm{VT},i}(t_k)$, respectively[2].

III. Position Estimation Approach

According to the description given in the previous section, an MPC can be represented by a direct path between a VT and the receiver plus an additional propagation length. However, the receiver position as well as the states of the VTs, i.e. $\boldsymbol{r}_{\mathrm{VT},i}(t_k)$ and $d_{\mathrm{VT},i}(t_k)$, are unknown. Additionally, it is unknown if the MPC is caused by a reflection or an interaction

[2]Please note, that the position of the VTs and the additional propagation lengths are constant over time. Nevertheless for notational convenience in the later sections a time dependence on t_k is introduced here.

with a scatterer. Hence, the state vector $\mathbf{x}(t_k)$ that describes the parameters to be estimated at time instant t_k for $N(t_k)$ MPCs is defined by

$$\mathbf{x}(t_k) = \left[\mathbf{x}_u(t_k)^T, \mathbf{x}_{\mathrm{VT}}(t_k)^T\right]^T, \quad (3)$$

with the receiver states

$$\mathbf{x}_u(t_k) = \left[\boldsymbol{r}_u(t_k)^T, \boldsymbol{v}_u(t_k)^T, b_u(t_k)\right]^T, \quad (4)$$

where $\boldsymbol{r}_u(t_k)$ is the receiver position, $\boldsymbol{v}_u(t_k)$ the receiver velocity, $b_u(t_k)$ the receiver's clock bias and the VT states

$$\mathbf{x}_{\mathrm{VT}}(t_k) = \left[\mathbf{x}_{\mathrm{VT},0}(t_k)^T, \ldots, \mathbf{x}_{\mathrm{VT},N(t_k)-1}(t_k)^T\right]^T. \quad (5)$$

The parameters representing the i-th VT are defined as

$$\mathbf{x}_{\mathrm{VT},i}(t_k) = \left[\boldsymbol{r}_{\mathrm{VT},i}(t_k)^T, d_{\mathrm{VT},i}(t_k)\right]^T, \quad (6)$$

where $\boldsymbol{r}_{\mathrm{VT},i}(t_k)$ is the position of the i-th VT and $d_{\mathrm{VT},i}(t_k)$ the additional propagation length. For notational conveniences, we use VT_0 to describe the physical transmitter with known $\boldsymbol{r}_{\mathrm{VT},0}(t_k) = \boldsymbol{r}_t$ and $d_{\mathrm{VT},0}(t_k) = 0$ in Section V-A and Section V-B.

Similarly to [33]–[36], the algorithm described in this paper is split into two levels: On the first level, the multipath parameters: amplitude $\alpha_i(t_k)$, AoA $\phi_i(t_k)$ and delay $\tau_i(t_k) = \frac{d_i(t_k)}{c}$ for each MPC $i = 0, \ldots, N(t_k) - 1$ are estimated based on the received signal $\boldsymbol{Y}(t_k)$. For consistency between different time instances, the multipath parameter estimation algorithm needs to include a path association such that distinct propagation paths are individually tracked over sequential time instances. In this paper, we use the algorithm called Kalman enhanced super resolution tracking (KEST), see [40], for the estimation and tracking of MPCs. Also other multipath estimation and tracking algorithms can be applied, e.g. [15], [41]. On the second level, Channel-SLAM recursively estimates the posterior distribution of the state vector $\mathbf{x}(t_k)$, $\mathsf{p}\big(\mathbf{x}(t_k)|\mathbf{Z}(t_{0:k})\big)$, using the parameters of all $N(t_k)$ MPCs as measurement $\mathbf{Z}(t_k)$, with

$$\mathbf{Z}(t_k) = [\hat{\boldsymbol{\phi}}(t_k),\ \hat{\mathbf{d}}(t_k)], \quad (7)$$

where

$$\hat{\boldsymbol{\phi}}(t_k) = [\hat{\phi}_0(t_k),\ \ldots\ , \hat{\phi}_{N(t_k)-1}(t_k)]^T \quad (8)$$

are the estimates for the AoA $\phi_i(t_k)$ and

$$\hat{\boldsymbol{d}}(t_k) = [\hat{d}_0(t_k),\ \ldots\ , \hat{d}_{N(t_k)-1}(t_k)]^T \quad (9)$$

are the estimates for the propagation path length $d_i(t_k) = \tau_i(t_k) \cdot c$ for the MPCs $i = 0 \ldots N(t_k) - 1$ with their corresponding variances $\boldsymbol{\Sigma}_z(t_k) = \left[\boldsymbol{\sigma}_d^2(t_k), \boldsymbol{\sigma}_\phi^2(t_k)\right]$. Multipath estimation algorithms like KEST cannot distinguish between reflected paths, scattered paths or the combination of both. However, by including the additional propagation length $d_{\mathrm{VT},i}(t_k)$ in the state vector $\mathbf{x}_{\mathrm{VT},i}(t_k)$, a specific model detection is not necessary, since for reflected paths, scattered paths or the combination of both, the same model can be used. Hence, if the MPC was interacting with a scatterer, Channel-SLAM estimates $d_{\mathrm{VT},i}(t_k) > 0$. If only reflections occurred on the pathway between physical transmitter and receiver, Channel-SLAM estimates $d_{\mathrm{VT},i}(t_k) \approx 0$. In this paper we concentrate on the derivation of Channel-SLAM, for a detailed description of multipath parameter estimation and tracking with KEST see [40] or similar types of algorithms in [15], [41].

A. Algorithm Description Based on Recursive Bayesian Filtering

Recursive Bayesian filtering provides a methodology to optimally estimate parameters in non-stationary conditions. The methodology consists of two steps, the prediction step to calculate $\mathsf{p}\big(\mathbf{x}(t_k)|\mathbf{Z}(t_{0:k-1})\big)$ and the update step to obtain $\mathsf{p}\big(\mathbf{x}(t_k)|\mathbf{Z}(t_{0:k})\big)$ which considers the measurement $\mathbf{Z}(t_k)$ at time instant t_k with the likelihood function $\mathsf{p}\big(\mathbf{Z}(t_k)|\mathbf{x}(t_k)\big)$ [42]. Assuming a first-order Markov model, the transition prior $\mathsf{p}\big(\mathbf{x}(t_k)|\mathbf{x}(t_{k-1})\big)$ used in the prediction step of the recursive Bayesian filter is defined here as

$$\mathsf{p}\big(\mathbf{x}(t_k)|\mathbf{x}(t_{k-1})\big) = \mathsf{p}\big(\mathbf{x}_u(t_k)|\mathbf{x}_u(t_{k-1})\big) \times \prod_{i=0}^{N(t_k)-1} \mathsf{p}\big(\mathbf{x}_{\mathrm{VT},i}(t_k)|\mathbf{x}_{\mathrm{VT},i}(t_{k-1})\big), \quad (10)$$

where we assume independence between the transition priors of the receiver state vector $\mathbf{x}_u(t_k)$ and the VT state vectors $\mathbf{x}_{\mathrm{VT},i}(t_k)$ associated to the MPCs $i = 0, \ldots, N(t_k)-1$. Please note that (10) inherently assumes independence among MPCs, i.e. propagation paths interact with distinct objects. This is based on the well-known uncorrelated scattering assumption in wireless propagation channel modelling [39]. As mentioned in Section II, the state $\mathbf{x}_{\mathrm{VT},i}(t_k)$ is time-invariant, hence, for the transition prior $\mathsf{p}\big(\mathbf{x}_{\mathrm{VT},i}(t_k)|\mathbf{x}_{\mathrm{VT},i}(t_{k-1})\big)$ of the i-th MPC we obtain

$$\mathsf{p}\big(\mathbf{x}_{\mathrm{VT},i}(t_k)|\mathbf{x}_{\mathrm{VT},i}(t_{k-1})\big) = \delta\left(\mathbf{x}_{\mathrm{VT},i}(t_k) - \mathbf{x}_{\mathrm{VT},i}(t_{k-1})\right). \quad (11)$$

For the transition prior $\mathsf{p}\big(\mathbf{x}_u(t_k)|\mathbf{x}_u(t_{k-1})\big)$ of the receiver state vector, i.e. the receiver position, velocity and clock bias, known prediction models can be applied[3], see e.g. [8], [43]–[45]. In this paper, we use a discrete time white noise acceleration model, see e.g. [45] with

$$\mathbf{x}_u(t_k) = \mathbf{A}_u(t_\delta)\mathbf{x}_u(t_{k-1}) + \mathbf{n}_u(t_k), \quad (12)$$

with the transition matrix

$$\mathbf{A}_u(t_\delta) = \begin{pmatrix} 1 & 0 & t_\delta & 0 & 0 \\ 0 & 1 & 0 & t_\delta & 0 \\ 0 & 0 & 1 & 0 & 0 \\ 0 & 0 & 0 & 1 & 0 \\ 0 & 0 & 0 & 0 & 1 \end{pmatrix}, \quad (13)$$

where $t_\delta = t_k - t_{k-1}$ defines the time between two adjacent time instants and $\mathbf{n}_u(t_k) \sim \mathcal{N}(0, \mathbf{Q}_u(t_\delta))$ defines the transi-

[3]Please note, if transmitter and receiver oscillators provide different frequencies, a clock drift parameter has to be considered additionally.

tion noise of the receiver state with

$$\mathbf{Q}_u(t_\delta)=\begin{pmatrix} \sigma_{q_u}^2\frac{(t_\delta)^3}{3} & 0 & \sigma_{q_u}^2\frac{(t_\delta)^2}{2} & 0 & 0 \\ 0 & \sigma_{q_u}^2\frac{(t_\delta)^3}{3} & 0 & \sigma_{q_u}^2\frac{(t_\delta)^2}{2} & 0 \\ \sigma_{q_u}^2\frac{(t_\delta)^2}{2} & 0 & \sigma_{q_u}^2 t_\delta & 0 & 0 \\ 0 & \sigma_{q_u}^2\frac{(t_\delta)^2}{2} & 0 & \sigma_{q_u}^2 t_\delta & 0 \\ 0 & 0 & 0 & 0 & \sigma_{q_b}^2 \end{pmatrix}, \tag{14}$$

where $\sigma_{q_u}^2$ defines the continuous-time process noise intensity, which has to be set based on the application with physical dimension $\left[\frac{\mathrm{m}^2}{\mathrm{s}^3}\right]$ and $\sigma_{q_b}^2$ the variance of the clock bias.

Assuming the elements of $\mathbf{Z}(t_k)$ to be independent Gaussian distributed conditioned on the current state $\mathbf{x}(t_k)$, $\mathsf{p}\big(\mathbf{Z}(t_k)|\mathbf{x}(t_k)\big)$ can be expressed as

$$\begin{aligned}\mathsf{p}\big(\mathbf{Z}(t_k)|\mathbf{x}(t_k)\big) = \prod_{i=0}^{N(t_k)-1} &\frac{1}{\sqrt{2\pi}\sigma_{d,i}(t_k)} e^{-\frac{(\hat{d}_i(t_k)-d_i(t_k))^2}{2\sigma_{d,i}^2(t_k)}} \\ &\times \frac{1}{\sqrt{2\pi}\sigma_{\phi,i}(t_k)} e^{-\frac{(\hat{\phi}_i(t_k)-\phi_i(t_k))^2}{2\sigma_{\phi,i}^2(t_k)}}, \end{aligned} \tag{15}$$

with the propagation length

$$d_i(t_k) = \|\boldsymbol{r}_u(t_k) - \boldsymbol{r}_{\mathrm{VT},i}(t_k)\| + d_{\mathrm{VT},i}(t_k) + b_u(t_k)\cdot c, \tag{16}$$

and the AoA

$$\phi_i(t_k) = \arccos\left(\frac{\left(\boldsymbol{r}_{\mathrm{VT},i}(t_k)-\boldsymbol{r}_u(t_k)\right)^T\cdot\boldsymbol{v}_u(t_k)}{\|\boldsymbol{r}_{\mathrm{VT},i}(t_k)-\boldsymbol{r}_u(t_k)\|\cdot\|\boldsymbol{v}_u(t_k)\|}\right), \tag{17}$$

for the i-th MPC, where $\sigma_{d,i}^2(t_k)$ and $\sigma_{\phi,i}^2(t_k)$ denote the corresponding variances. Please note that we assume in (17) that the linear antenna array is aligned to the direction of $\boldsymbol{v}_u(t_k)$, i.e. the moving direction.

B. Rao-Blackwellized Particle Filter (RBPF)

In this section a formulation of Channel-SLAM is derived based on Rao-Blackwellization, where the states space of $\mathbf{x}(t_k)$ is partitioned into subspaces, see [37], [46]. Hence, we use PFs to estimate the subspaces representing the VTs inside a PF. The formulation allows to use different numbers of particles in each PF associated to a VT and reduces the computational complexity compared to [33]–[35]. The reason to use a PF instead of a low complexity EKF is the high nonlinearity of the measurements in (17) and (16). Assuming the independency in (10), the posterior density $\mathsf{p}\big(\mathbf{x}(t_{0:k})|\mathbf{Z}(t_{0:k})\big)$ is written as

$$\begin{aligned}&\mathsf{p}\big(\mathbf{x}(t_{0:k})|\mathbf{Z}(t_{0:k})\big) \\ &= \mathsf{p}\big(\mathbf{x}_u(t_{0:k}), \mathbf{x}_{\mathrm{VT}}(t_{0:k})|\mathbf{Z}(t_{0:k})\big) \\ &= \mathsf{p}\big(\mathbf{x}_u(t_{0:k})|\mathbf{Z}(t_{0:k})\big)\cdot\mathsf{p}\big(\mathbf{x}_{\mathrm{VT}}(t_{0:k})|\mathbf{x}_u(t_{0:k}), \mathbf{Z}(t_{0:k})\big) \\ &= \mathsf{p}\big(\mathbf{x}_u(t_{0:k})|\mathbf{Z}(t_{0:k})\big) \\ &\quad\times\prod_{i=0}^{N(t_k)-1}\mathsf{p}\big(\mathbf{x}_{\mathrm{VT},i}(t_{0:k})|\mathbf{x}_u(t_{0:k}), \mathbf{z}_i(t_{0:k})\big),\end{aligned} \tag{18}$$

where $\mathbf{z}_i(t_k)$ denotes the measurements of the i-th MPC with $\mathbf{z}_i(t_k) = \left[\hat{\phi}_i(t_k), \hat{d}_i(t_k)\right]^T$. In (18) we assume independency between the state vectors of the individual MPCs. Due to using a first order hidden Markov model, only the estimated posterior filtered density $\mathsf{p}\big(\mathbf{x}(t_k)|\mathbf{Z}(t_{0:k})\big)$ at time instant t_k is required for the next time instant t_{k+1}. As shown in Fig. 2, the algorithm is based on a superordinate particle filter (superPF) and subordinate particle filters (subPFs): Each particle $j = 1\dots N_s$ of the superPF with the state vector $\mathbf{x}_u^{(j)}(t_k) = \left[\boldsymbol{r}_u^{(j)}(t_k)^T, \boldsymbol{v}_u^{(j)}(t_k)^T, b_u^{(j)}(t_k)\right]^T$ consists of $N(t_k)$ subPFs. Each subPF is represented by the particles $\mathbf{x}_{\mathrm{VT},i}^{(j,a)}(t_k)$ with $a = 1,\dots,N_{P,j,i}$ where $N_{P,j,i}$ stands for the number of particles in the i-th subPF with $i = 0,\dots,N(t_k)-1$, estimating $\mathbf{x}_{\mathrm{VT},i}^{(j)}(t_k)$. In the superPF, the marginalized posterior filtered density $\mathsf{p}\big(\mathbf{x}_u(t_k)|\mathbf{Z}(t_{0:k})\big)$ can be approximated by importance samples, see [42], as

$$\begin{aligned}&\mathsf{p}\big(\mathbf{x}_u(t_k)|\mathbf{Z}(t_{0:k})\big) \\ &\quad\approx \sum_{j=1}^{N_s} w^{(j)}(t_k)\,\delta\left(\mathbf{x}_u(t_k)-\mathbf{x}_u^{(j)}(t_k)\right),\end{aligned} \tag{19}$$

where $w^{(j)}(t_k)$ defines the weight for the j-th particle at time instant t_k. Using the transition prior $\mathsf{p}\big(\mathbf{x}_u(t_k)|\mathbf{x}_u(t_{k-1})\big)$ as the importance density [37], [46], the weight $w^{(j)}(t_k)$ can be calculated recursively by

$$\begin{aligned}&w^{(j)}(t_k) \\ &\propto\ w^{(j)}(t_{k-1})\cdot\mathsf{p}\big(\mathbf{Z}(t_k)|\mathbf{x}_u^{(j)}(t_k), \mathbf{Z}(t_{k-1})\big) \\ &\propto\ w^{(j)}(t_{k-1})\int\mathsf{p}\big(\mathbf{Z}(t_k)|\mathbf{x}_u^{(j)}(t_k), \mathbf{x}_{\mathrm{VT}}(t_k), \mathbf{Z}(t_{k-1})\big) \\ &\qquad\times\mathsf{p}\big(\mathbf{x}_{\mathrm{VT}}(t_k)|\mathbf{x}_u^{(j)}(t_k), \mathbf{Z}(t_{k-1})\big)\ \mathrm{d}\mathbf{x}_{\mathrm{VT}}(t_k) \\ &\propto\ w^{(j)}(t_{k-1}) \\ &\qquad\times\prod_{i=0}^{N(t)-1}\int\mathsf{p}\big(\mathbf{z}_i(t_k)|\mathbf{x}_u^{(j)}(t_k), \mathbf{x}_{\mathrm{VT},i}(t_k), \mathbf{z}_i(t_{k-1})\big) \\ &\qquad\times\mathsf{p}\big(\mathbf{x}_{\mathrm{VT},i}(t_k)|\mathbf{x}_u^{(j)}(t_k), \mathbf{z}_i(t_{k-1})\big)\ \mathrm{d}\mathbf{x}_{\mathrm{VT},i}(t_k),\end{aligned} \tag{20}$$

again with the assumption of independency among MPCs. The term $\mathsf{p}\big(\mathbf{x}_{\mathrm{VT},i}(t_k)|\mathbf{x}_u^{(j)}(t_k), \mathbf{z}_i(t_{k-1})\big)$ of (20) can be reformulated to

$$\begin{aligned}&\mathsf{p}\big(\mathbf{x}_{\mathrm{VT},i}(t_k)|\mathbf{x}_u^{(j)}(t_k), \mathbf{z}_i(t_{k-1})\big) \\ &=\int\mathsf{p}\big(\mathbf{x}_{\mathrm{VT},i}(t_k)|\mathbf{x}_{\mathrm{VT},i}(t_{k-1}), \mathbf{x}_u^{(j)}(t_k), \mathbf{z}_i(t_{k-1})\big) \\ &\quad\times\mathsf{p}\big(\mathbf{x}_{\mathrm{VT},i}(t_{k-1})|\mathbf{x}_u^{(j)}(t_k), \mathbf{z}_i(t_{k-1})\big)\,\mathrm{d}\mathbf{x}_{\mathrm{VT},i}(t_{k-1}).\end{aligned} \tag{21}$$

In order to calculate (21), we consider the stationarity of the VTs for all time instants of (11) and that the states of the VTs $\mathbf{x}_{\mathrm{VT},i}(t_{k-1})$ are independent from the receiver states $\mathbf{x}_u^{(j)}(t_k)$ accoding to (10), hence,

$$\begin{aligned}&\mathsf{p}\big(\mathbf{x}_{\mathrm{VT},i}(t_k)|\mathbf{x}_{\mathrm{VT},i}(t_{k-1}), \mathbf{x}_u^{(j)}(t_k), \mathbf{z}_i(t_{k-1})\big) \\ &\qquad= \mathsf{p}\big(\mathbf{x}_{\mathrm{VT},i}(t_k)|\mathbf{x}_{\mathrm{VT},i}(t_{k-1})\big) \\ &\qquad= \delta\left(\mathbf{x}_{\mathrm{VT},i}(t_k)-\mathbf{x}_{\mathrm{VT},i}(t_{k-1})\right),\end{aligned} \tag{22}$$

and represent $\mathsf{p}\big(\mathbf{x}_{\mathrm{VT},i}(t_{k-1})|\mathbf{x}_u^{(j)}(t_k), \mathbf{z}_i(t_{k-1})\big)$ by $N_{P,i,j}$ Kernels $\mathrm{K}(\cdot)$ with weight $w_i^{(j,a)}(t_{k-1})$ and bandwith

$\sigma_{\mathrm{K},i}^{(j)}(t_{k-1})$, which is a regularized PF [42], thus,

$$\begin{aligned}&\mathsf{p}\big(\mathbf{x}_{\mathrm{VT},i}(t_{k-1})|\mathbf{x}_u^{(j)}(t_k)\,,\mathbf{z}_i(t_{k-1})\big) \\ &\quad=\sum_{a=1}^{N_{P,i,j}} w_i^{(j,a)}(t_{k-1})\cdot \mathrm{K}(\mathbf{x}_{\mathrm{VT},i}(t_{k-1})-\mathbf{x}_{\mathrm{VT},i}^{(j,a)}(t_{k-1})).\end{aligned} \tag{23}$$

Hence, we obtain from (21) by inserting (22) and (23)

$$\begin{aligned}&\mathsf{p}\big(\mathbf{x}_{\mathrm{VT},i}(t_k)|\mathbf{x}_u^{(j)}(t_k)\,,\mathbf{z}_i(t_{k-1})\big) \\ &\quad\approx\sum_{a=1}^{N_{P,i,j}} w_i^{(j,a)}(t_{k-1})\cdot \mathrm{K}(\mathbf{x}_{\mathrm{VT},i}(t_k)-\mathbf{x}_{\mathrm{VT},i}^{(j,a)}(t_{k-1})).\end{aligned} \tag{24}$$

Finally, we obtain from (20) by inserting (24)

$$\begin{aligned}w^{(j)}(t_k) \;&\propto\; w^{(j)}(t_{k-1})\prod_{i=0}^{N(t)-1}\sum_{a=1}^{N_{P,i,j}} w_i^{(j,a)}(t_{k-1}) \\ &\quad\int \mathsf{p}\big(\mathbf{z}_i(t_k)|\mathbf{x}_u^{(j)}(t_k)\,,\mathbf{x}_{\mathrm{VT},i}(t_k)\big) \\ &\quad\times\mathrm{K}(\mathbf{x}_{\mathrm{VT},i}(t_k)-\mathbf{x}_{\mathrm{VT},i}^{(j,a)}(t_{k-1}))\,\mathrm{d}\mathbf{x}_{\mathrm{VT},i}(t_k) \\ &\propto\; w^{(j)}(t_{k-1})\prod_{i=0}^{N(t)-1}\sum_{a=1}^{N_{P,i,j}} \\ &\quad\underbrace{w_i^{(j,a)}(t_{k-1})\mathsf{p}\big(\mathbf{z}_i(t_k)|\mathbf{x}_u^{(j)}(t_k)\,,\mathbf{x}_{\mathrm{VT},i}^{(j,a)}(t_k)\big)}_{w_i^{(j,a)}(t_k)}\end{aligned} \tag{25}$$

where we use $\mathsf{p}\big(\mathbf{z}_i(t_k)|\mathbf{x}_u^{(j)}(t_k)\,,\mathbf{x}_{\mathrm{VT},i}(t_k)\big) = \mathsf{p}\big(\mathbf{z}_i(t_k)|\mathbf{x}_u^{(j)}(t_k)\,,\mathbf{x}_{\mathrm{VT},i}(t_k)\,,\mathbf{x}_{\mathrm{VT},i}^{(j,a)}(t_{k-1})\big)$ and interprete $\mathrm{K}(\mathbf{x}_{\mathrm{VT},i}(t_k)-\mathbf{x}_{\mathrm{VT},i}^{(j,a)}(t_{k-1}))$ as a density given the particle state $\mathbf{x}_{\mathrm{VT},i}^{(j,a)}(t_{k-1})$ and using $\mathbf{x}_{\mathrm{VT},i}^{(j,a)}(t_k)=\mathbf{x}_{\mathrm{VT},i}^{(j,a)}(t_{k-1})$. Hence, the weight $w_i^{(j,a)}(t_k)$ of the subPFs at time instant t_k is

$$w_i^{(j,a)}(t_k)\triangleq w_i^{(j,a)}(t_{k-1})\cdot\mathsf{p}\big(\mathbf{z}_i(t_k)|\mathbf{x}_u^{(j)}(t_k)\,,\mathbf{x}_{\mathrm{VT},i}^{(j,a)}(t_k)\big). \tag{26}$$

C. RBPF Implementation

Algorithm 1 provides the pseudocode of Channel-SLAM, which is executed at every time instant $t_k \geq t_0$ with the estimates $\mathbf{Z}(t_k)\,,\boldsymbol{\Sigma}_z(t_k)$ obtained from KEST. During the initialization, at time instant $t_k=t_0$, the particles $\{\mathbf{x}_u^{(j)}(t_0)\}_{j=1}^{N_s}$ of the superPF are initialized according to prior knowledge. The particles $\{\mathbf{x}_{\mathrm{VT},i}^{(j,a)}(t_0)\}_{a=1}^{N_{p,j,i}}$ of the subPFs are initialized dependent on $\mathbf{x}_u^{(j)}(t_0)$ and the measurements $\hat{d}_i(t_0),\hat{\phi}_i(t_0)$ for the i-th MPC. To initialize the states of $\mathbf{x}_{\mathrm{VT},i}^{(j,a)}(t_0)$ with $a=1,\ldots,N_{p,j,i}$ of the j-th subPF associated to the i-th MPC a grid is used. The positions $\mathbf{r}_{\mathrm{VT},i}^{(j,a)}(t_0)$ of the particles $\{\mathbf{x}_{\mathrm{VT},i}^{(j,a)}(t_0)\}_{a=1}^{N_{P,j,i}}$ are distributed such that

$$0\leq\|\mathbf{r}_{\mathrm{VT},i}^{(j,a)}(t_0)-\boldsymbol{r}_u^{(j)}(t_0)\|\leq\hat{d}_i(t_0)+\Delta_d \tag{27}$$

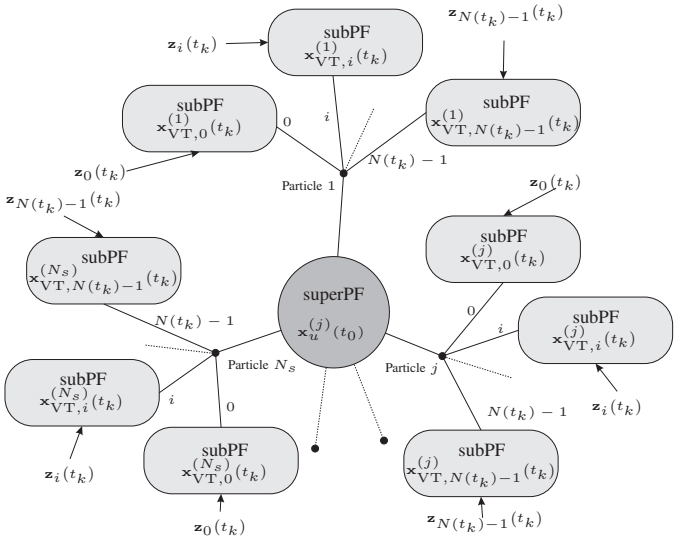

Fig. 2. The algorithm is based on a superordinate particle filter (superPF) and subordinate particle filters (subPFs): the subPFs estimate the conditional posterior density $\mathsf{p}\big(\mathbf{x}_{\mathrm{VT},i}(t_k)|\mathbf{x}_u(t_k)\,,\mathbf{z}_i(t_{0:k})\big)$ of $\mathbf{x}_{\mathrm{VT},i}(t_k)$ for the i-th VT and the superPF estimates the marginalized posterior filtered density $\mathsf{p}\big(\mathbf{x}_u(t_k)|\mathbf{Z}(t_{0:k})\big)$ of $\mathbf{x}_u(t_k)$. Each particle $j=1\ldots N_s$ of the superPF consists of $N(t_k)$ subPFs.

with spacing Δ_d, hence, $N_{d,i}=\lfloor\frac{\hat{d}_i(t_0)}{\Delta_d}\rfloor+1$ grid points and

$$\begin{aligned}&\hat{\phi}_i(t_0)-K\cdot\sigma_{\phi,i}(t_0) \\ &\quad\leq\arccos\left(\frac{\big(\mathbf{r}_{\mathrm{VT},i}^{(j,a)}(t_0)-\boldsymbol{r}_u^{(j)}(t_0)\big)\cdot\boldsymbol{v}_u^{(j)}(t_0)}{\|\mathbf{r}_{\mathrm{VT},i}^{(j,a)}(t_0)-\boldsymbol{v}_u^{(j)}(t_0)\|\cdot\|\boldsymbol{v}_u^{(j)}(t_0)\|}\right)\leq \\ &\qquad\hat{\phi}_i(t_0)+K\cdot\sigma_{\phi,i}(t_0)\end{aligned} \tag{28}$$

with spacing Δ_ϕ, resulting in $N_{\phi,i}=\lfloor\frac{2K\cdot\sigma_{\phi,i}}{\Delta_\phi}\rfloor+1$ grid points, where K denotes an empirical constant value. The additional propagation length is $d_{\mathrm{VT},i}^{(j,a)}(t_0)=\hat{d}_i(t_0)-\|\mathbf{r}_{\mathrm{VT},i}^{(j,a)}(t_0)-\boldsymbol{r}_u^{(j)}(t_0)\|$, where we inherently assume $b_u(t_0)=0$ for the initialization. Hence, the total number of particles can be calculated as

$$N_{\mathrm{t}}=\sum_{j=1}^{N_p}\sum_{i=0}^{N(t_k)-1}N_{P,j,i}=N_p\sum_{i=0}^{N(t_k)-1}N_{d,i}\cdot N_{\phi,i}. \tag{29}$$

The number of detected MPCs may change, hence, Channel-SLAM determines at each time instant whether the number of tracked MPCs has changed. In case that new MPCs have been detected, new subPFs are added and initialized using (27) and (28) (cf. Line 7 in Algorithm 1). In case that MPCs are not tracked by KEST anymore, the corresponding subPFs are removed (cf. Line 9 in Algorithm 1). Neither KEST nor Channel-SLAM consider re-tracking of previous MPCs. Hence, if the tracking of an MPC has been lost and might be regained, the corresponding VT is initialized without any prior information. According to (11) the state $\mathbf{x}_{\mathrm{VT},i}(t_k)$ is time-invariant, hence each subPF assigns the states of the VTs with $\mathbf{x}_{\mathrm{VT},i}^{(j,a)}(t_k)=\mathbf{x}_{\mathrm{VT},i}^{(j,a)}(t_{k-1})$ and calculates the weight $w_i^{(j,a)}(t_k)$ using (26). Thereafter, the weight $w^{(j)}(t_k)$ is calculated using (25) (cf. Line 15 in Algorithm 1). Afterwards, the subPFs and superPF are resampled, weights are normalized

(cf. Line 16 in Algorithm 1), see [42], [43], [47], and the states of the VTs $\mathbf{x}_{\mathrm{VT},i}^{(j,a)}(t_k)$ are drawn using a Gaussian-Kernel (cf. Line 19 in Algorithm 1).

The point estimate, $\hat{\mathbf{x}}(t_k) = \left[\hat{\mathbf{x}}_u(t_k)^T, \hat{\mathbf{x}}_{\mathrm{VT}}(t_k)^T\right]^T$ (cf. Line 20 in Algorithm 1) is calculated according to the minimum mean square error (MMSE) criterion. The MMSE of the RBPF can be derived with (25) as (30).

Algorithm 1: Channel-SLAM for time instant t_k

Input:
Multipath estimates: $\mathbf{Z}(t_k)$ and $\mathbf{\Sigma}_z(t_k)$
States of subPFs and superPF:
$\{\{\mathbf{x}_{\mathrm{VT},i}^{(j,a)}(t_{k-1})\}_{a=1}^{N_{p,j,i}}\}_{j=1}^{N_s}$, $\{\mathbf{x}_u^{(j)}(t_{k-1})\}_{j=1}^{N_s}$ for $t_k > t_0$
Weights of subPFs and superPF:
$\{\{w_i^{(j,a)}(t_{k-1})\}_{a=1}^{N_{p,j,i}}\}_{j=1}^{N_s}$, $\{w^{(j)}(t_{k-1})\}_{j=1}^{N_s}$ for $t_k > t_0$
Output:
States of subPFs and superPF:
$\{\{\mathbf{x}_{\mathrm{VT},i}^{(j,a)}(t_k)\}_{a=1}^{N_{p,j,i}}\}_{j=1}^{N_s}$, $\{\mathbf{x}_u^{(j)}(t_k)\}_{j=1}^{N_s}$ for $t_k \geq t_0$
Weights of subPFs and superPF:
$\{\{w_i^{(j,a)}(t_k)\}_{a=1}^{N_{p,j,i}}\}_{j=1}^{N_s}$, $\{w^{(j)}(t_k)\}_{j=1}^{N_s}$ for $t_k > t_0$
MMSE estimate: $\hat{\mathbf{x}}(t_k)$ for $t_k > t_0$

1 **if** $t_k = t_0$ **then**
2 Initialization using $\mathbf{Z}(t_0)$ and $\mathbf{\Sigma}_z(t_0)$;
3 **else**
4 **for** $j = 1 : N_s$ **do**
5 Draw $\mathbf{x}_u^{(j)}(t_k) \sim \mathsf{p}\big(\mathbf{x}_u^{(j)}(t_k)|\mathbf{x}_u^{(j)}(t_{k-1})\big)$;
6 **if** *New paths detected* **then**
7 Initialize new subPFs;
8 **if** *Tracking of paths lost* **then**
9 Delete corresponding subPFs;
10 **for** $i = 0 : N(t_k) - 1$ **do**
11 **for** $a = 1 : N_{P,j,i}$ **do**
12 Assign $\mathbf{x}_{\mathrm{VT},i}^{(j,a)}(t_k) = \mathbf{x}_{\mathrm{VT},i}^{(j,a)}(t_{k-1})$;
13 Calculate $w_i^{(j,a)}(t_k) = w_i^{(j,a)}(t_{k-1})\mathsf{p}\big(\mathbf{z}_i(t_k)|\mathbf{x}_u^{(j)}(t_k), \mathbf{x}_{\mathrm{VT},i}^{(j,a)}(t_k)\big)$;
14 Calculate total subPF weight: $t_{j,i} = \mathrm{SUM}[\{w_i^{(j,a)}(t_k)\}_{a=1}^{N_{P,j,i}}]$;
15 $w^{(j)}(t_k) = w^{(j)}(t_{k-1}) \prod_{i=0}^{N(t_k)-1} t_{j,i}$;
16 Normalize and Resample subPFs and superPF;
17 **for** $i = 0 : N(t_k) - 1$ **do**
18 **for** $a = 1 : N_{P,j,i}$ **do**
19 Draw $\mathbf{x}_{\mathrm{VT},i}^{(j,a)}(t_k)$ from the Gaussian-Kernel;
20 Calculate MMSE $\hat{\mathbf{x}}(t_k)$ according to (30);

IV. Posterior Cramér-Rao Lower Bound

The PCRLB can be calculated by the inverse of the posterior Fisher information matrix $\mathbf{J}(t_k)$ and provides a lower bound of the variance of a Bayesian estimator [48] with

$$\mathbf{E}\left[\|\hat{\mathbf{x}}(t_k) - \mathbf{x}(t_k)\|^2\right] \geq \mathrm{PCRLB}\left[\mathbf{x}(t_k)\right] = \mathbf{J}(t_k)^{-1}. \quad (31)$$

To consider a dynamic system in the PCRLB, the state transition from time instant t_{k-1} to time instant t_k can be obtained by combining the time-invariant transition model for $\mathbf{x}_{\mathrm{VT},i}(t_k)$ as introduced in (11) for the VTs and the transition matrix for the receiver as introduced in (13) with

$$\mathbf{x}(t_k) = \underbrace{\begin{pmatrix} \mathbf{A}_u(t_\delta) & \mathbf{0} \\ \mathbf{0} & \mathbf{I} \end{pmatrix}}_{\mathbf{A}(t_\delta)} \mathbf{x}(t_{k-1}) + \begin{pmatrix} \mathbf{n}_u(t_k) \\ \mathbf{0} \end{pmatrix} \quad (32)$$

where $\mathbf{n}_u(t_k) \sim \mathcal{N}(0, \mathbf{Q}_u(t_\delta))$ describes the system noise of the user state, see (14). According to [49] by using the matrix inversion lemma, the posterior Fisher information can be calculated recursively by

$$\mathbf{J}(t_k) = \mathbf{R}(t_k) + \left(\mathbf{Q}(t_\delta) + \mathbf{A}(t_\delta)\mathbf{J}(t_{k-1})^{-1}\mathbf{A}(t_\delta)^T\right)^{-1}, \quad (33)$$

where $\mathbf{R}(t_k)$ is the snapshot based Fisher information matrix and the covariance matrix

$$\mathbf{Q}(t_\delta) = \begin{pmatrix} \mathbf{Q}_u(t_\delta) & \mathbf{0} \\ \mathbf{0} & \mathbf{0} \end{pmatrix}. \quad (34)$$

Here, the PCRLB considers the complete system, including both levels, i.e. the multipath parameter estimation and Channel-SLAM. In general, a two level approach performs either equally or worse than an estimator which jointly combines both levels. Hence, the derived PCRLB is based on a theoretical joint approach and consideres therefore, the best possible estimator. In (2), we consider $N(t_k)$ received MPCs with $b_l(\phi_i(t_k)) = e^{-j2\pi f_c \tau_{i,l}(t_k)}$ where $\tau_{i,l}$ is the delay of the i-th MPC for the l-th antenna element $l = 1 \ldots L$. Therefore, the discrete channel transfer function in dependence on $\mathbf{x}(t_k)$ can be written as

$$\mu(\omega_m, l; \mathbf{x}(t_k)) = \sum_{i=0}^{N(t_k)-1} \alpha_{i,l}(t_k) e^{-j(2\pi f_c + \omega_m)\, \tau_{i,l}(t_k)} \quad (35)$$

where f_c is the carrier frequency, ω_m defines the discrete circular frequency at index $m = 0 \ldots M-1$ and $\alpha_{i,l}(t_k)$ the complex amplitude of the i-th MPC. According to the system model in (16), the delay of the i-th MPC is

$$\tau_{i,l}(t_k) = \left(\|\tilde{\mathbf{d}}_{\mathrm{VT},i,l}(t_k)\| + d_{\mathrm{VT},i}(t_k)\right)\frac{1}{c} + b_u(t_k), \quad (36)$$

with

$$\tilde{\mathbf{d}}_{\mathrm{VT},i,l}(t_k) = \boldsymbol{r}_{\mathrm{VT},i}(t_k) - \left(\boldsymbol{r}_u(t_k) + \frac{\boldsymbol{v}_u(t_k) \cdot (l-1) \cdot d}{\|\boldsymbol{v}_u(t_k)\|}\right) \quad (37)$$

where d defines the spacing between adjacent antennas. The snapshot based Fisher information matrix $\mathbf{R}(t_k)$ in (33) can be obtained by

$$[\mathbf{R}(t_k)]_{k,w} = \frac{2}{\sigma_n^2} \Re\left\{\frac{\partial \boldsymbol{\mu}(\mathbf{x}(t_k))^H}{\partial [\mathbf{x}(t_k)]_k} \frac{\partial \boldsymbol{\mu}(\mathbf{x}(t_k))}{\partial [\mathbf{x}(t_k)]_w}\right\}, \quad (38)$$

where

$$\boldsymbol{\mu}(\mathbf{x}(t_k)) = [\mu(\omega_0, 1; \mathbf{x}(t_k)), \ldots, \mu(\omega_0, L; \mathbf{x}(t_k)), \ldots, \mu(\omega_{M-1}, 1; \mathbf{x}(t_k)), \ldots, \mu(\omega_{M-1}, L; \mathbf{x}(t_k))]^T.$$

$$\hat{\mathbf{x}}(t_k) = \int_{\mathbf{x}_u(t_k)} \int_{\mathbf{x}_{\mathrm{VT}}(t_k)} \mathbf{x}(t_k)\, \mathsf{p}\big(\mathbf{x}_u(t_k), \mathbf{x}_{\mathrm{VT}}(t_k) | \mathbf{Z}(t_k)\big)\, \mathrm{d}\mathbf{x}_u(t_k)\ \mathrm{d}\mathbf{x}_{\mathrm{VT}}(t_k)$$
$$\approx \sum_{j=1}^{N_s} w^{(j)}(t_k) \begin{bmatrix} \mathbf{x}_u^{(j)}(t_k) \\ \sum_{a=1}^{N_{P,j,0}} w_0^{(j,a)}(t_k) \mathbf{x}_{\mathrm{VT},0}^{(j,a)}(t_k) \\ \vdots \\ \sum_{a=1}^{N_{P,j,N(t_k)-1}} w_{N(t_k)-1}^{(j,a)}(t_k) \mathbf{x}_{\mathrm{VT},N(t_k)-1}^{(j,a)}(t_k) \end{bmatrix} \tag{30}$$

The derivatives of $\boldsymbol{\mu}(\mathbf{x}(t_k))$ with respect to the elements of the state vector $\mathbf{x}(t_k)$ are derived in the Appendix.

V. Performance Evaluations

This section evaluates the performance of Channel-SLAM based on artificial simulations in Section V-A and measurements in Section V-B where both evaluations include a LoS to NLoS transition.

A. Simulation Results

In this section, we evaluate the performance of Channel-SLAM using a two dimensional scenario with a static transmitter, a moving receiver, a reflecting surface and a scatterer, shown in Fig. 3. The receiver is moving on a random pathway for 20 s with a system sampling interval of $t_\delta = 0.1$ s. The receiver is equipped with a 3-element linear antenna array with an element-spacing of 0.5λ, where the wave length $\lambda = c/f_c \approx 0.2$ m with $f_c = 1.51$ GHz, which is aligned to the direction of movement. During the receiver movement, the LoS path between transmitter and receiver is present for $t_k \leq 10$ s and has a normalized amplitude of 1. For $10\,\mathrm{s} < t_k \leq 20\,\mathrm{s}$, the transmitter and receiver are in NLoS conditions and only MPCs are received. During the whole receiver movement, the signal reaches the receiving antenna via four different propagation paths at each time instant t_k: a reflected path with normalized amplitude of $1/2$ associated to VT_1, a scattered path with normalized amplitude of $1/3$ associated to VT_2, a path which is first reflected and afterwards scattered with normalized amplitude of $1/4$ associated to VT_3 and a path which is first scattered and afterwards reflected with normalized amplitude of $1/6$ associated to VT_4. The band-unlimited CIRs for each time instant t_k are bandlimited to a bandwidth of 100 MHz. The simulations are performed for different signal-to-noise-ratios (SNRs) which are calculated as $\mathrm{SNR} = \frac{\|\tilde{\mathbf{Y}}(t_k)^2\|}{L\,M\,\sigma_n^2}$, where $\|\tilde{\mathbf{Y}}(t_k)\|^2$ is the power of all paths' contributions $\tilde{\mathbf{Y}}(t_k)$, see (2). For the simulations, the clock bias is drawn randomly for each Monte-Carlo run. As mentioned in the previous sections, the VT position of the reflected signal path is determined by mirroring the transmitter at the reflecting surface, indicated by VT_1 in Fig. 3 with $d_{\mathrm{VT},1} = 0$. The position of the scatterer is equivalent to the position of VT_2 and VT_3 with $d_{\mathrm{VT},2} = \|\boldsymbol{r}_t - \boldsymbol{r}_s\| = 8.6$ m and $d_{\mathrm{VT},3} = \|\boldsymbol{r}_{\mathrm{VT},1} - \boldsymbol{r}_s\| = 22.1$ m, respectively. The position of VT_4 can be determined by mirroring the scatterer at the reflecting surface with the additional propagation length $d_{\mathrm{VT},4} = d_{\mathrm{VT},2}$. Fig. 3 visualizes these propagation paths for a receiver at the end of the track. Please note that at time instant $t_k = 14.2$ s the delay of the paths associated to VT_3 and VT_4 are equal. However, because of different amplitudes, phases and AoAs of these MPCs, KEST is able to track both paths separately, see also [40].

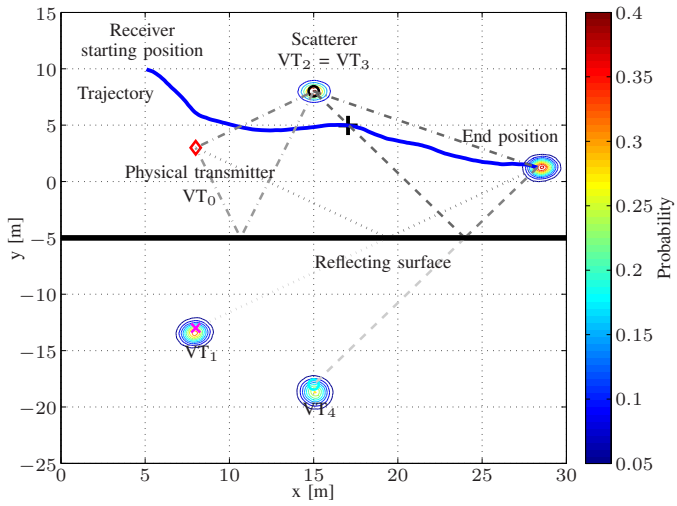

Fig. 3. Simulated scenario with a fixed physical transmitter, a moving receiver, a reflecting surface and a scatterer. The signal reaches the receiving antenna via five different propagation paths: the LoS path for $0\,\mathrm{s} \leq t_k \leq 10\,\mathrm{s}$, a reflected path, a path which is scattered, a path which is first reflected and afterwards scattered and a path which is scattered and afterwards reflected. The black circle, the purple cross and the light blue circle represent the true positions of VT_1, VT_2, VT_3 and VT_4, respectively. Additionally, the figure shows the PDFs of the estimated VT positions and the receiver position at time instant $t_k = 20$ s for SNR = 24 dB using a contour plot. The black cross indicates the receiver position at $t_k = 10$ s.

To verify the estimation performance of Channel-SLAM, KEST is used with a fixed model order of $N(t_k) = 5$ for $0\,\mathrm{s} \leq t_k \leq 10\,\mathrm{s}$ and $N(t_k) = 4$ for $10\,\mathrm{s} < t_k \leq 20\,\mathrm{s}$. The simulations are performed using $N_s = 6000$ particles in the superPF, whereas the number of particles for the subPFs for each MPC with $i = 0, \ldots, 4$ is different depending on the estimated delay and AoA of each MPC. As mentioned in Section III we consider for conveniences the first MPC $i = 0$ as the LoS path, indicated by VT_0 in Fig. 3 with a known fixed position $\boldsymbol{r}_{\mathrm{VT},0}(t_k) = \boldsymbol{r}_t$ and $d_{\mathrm{VT},0}(t_k) = 0$. For the initialization of Channel-SLAM, we use prior information $\mathsf{p}\big(\mathbf{x}_u(t_0)\big)$. The prior information includes a uniform distribution of 1 m width centered around the starting position for $\boldsymbol{r}_u(t_0)$. Additionally, the speed vector $\|\boldsymbol{v}_u(t_0)\|$ is initialized

in terms of speed using a uniform distribution between $0\,\mathrm{m/s}$ and $2\,\mathrm{m/s}$ and a uniform direction of $60°$ width around the true moving direction. Please note, that an unknown starting position and direction or larger initial uncertainties may result in a biased and rotated coordinate system for the estimation. For Δ_d, Δ_ϕ, K, we use empirical values as $\Delta_d = 0.1\,\mathrm{m}, \Delta_\phi = 0.5°, K = 5$.

Fig. 4 shows the root mean square error (RMSE) versus different SNRs for the receiver and VT positions at the end of the track, i.e. $t_k = 20\,\mathrm{s}$. The green solid curve represents the $\mathrm{RMSE}_u(t_k) = \sqrt{\mathbf{E}\{\|\boldsymbol{r}_u(t_k) - \hat{\boldsymbol{r}}_u(t_k)\|^2\}}$ of the estimated user position, the magenta, yellow, blue and orange the $\mathrm{RMSE}_{\mathrm{VT},i}(t_k) = \sqrt{\mathbf{E}\{\|\boldsymbol{r}_{\mathrm{VT},i}(t_k) - \hat{\boldsymbol{r}}_{\mathrm{VT},i}(t_k)\|^2\}}$ of the estimated i-th VT position and in cyan the error of the clock bias estimation times the speed of light in meters, $\mathrm{RMSE}_b(t_k) = \sqrt{\mathbf{E}\{\|b_u(t_k) - \hat{b}_u(t_k)\|^2\}} \cdot c$. Whereas the solid lines indicate the RMSE for the simulations, the dashed lines indicate the corresponding curves calculated using the PCRLB. Because the positions of VT_2 and VT_3 are identical, the curves for the PCRLBs of these VTs are equivalent. For low SNRs, it is difficult for KEST to accurately estimate all five paths due to poor initialization caused by noise. Hence, also Channel-SLAM does a wrong initialization and estimation of these VTs which causes high position errors for low SNRs. For SNR $\leq 6\,\mathrm{dB}$, the $\mathrm{RMSE}_{\mathrm{VT},2}(t_k)$ is larger than $\mathrm{RMSE}_{\mathrm{VT},3}(t_k)$ due to the higher received power of the path associated to VT_2 compared to VT_3. For higher SNRs, the RMSEs for VT_2 and VT_3 are close to the curves for the PCRLBs. Furthermore, for SNRs higher than $20\,\mathrm{dB}$ the receiver is able to estimate the receiver position with a RMSE below $0.3\,\mathrm{m}$. Because VT_2 and VT_3 are closer to the track than VT_1 and VT_4, the delay and AoA are changing more significantly, hence, the parameter estimations of VT_2 and VT_3 are more accurate. The precise estimation of the receiver and VT positions is also shown in Fig. 3, which shows the PDFs of the estimated VT positions and the receiver position at the end of the track, i.e. $t_k = 20\,\mathrm{s}$, for SNR = 24 dB.

To see the positioning performance of Channel-SLAM in relation to other algorithms, Fig. 5 compares Channel-SLAM to four different algorithms named as Alg. I to Alg. IV.

- **Alg. I**: Positioning algorithm with perfect knowledge of all VT positions $\boldsymbol{r}_{\mathrm{VT},i}(t_k)$ and additional propagation lengths $d_{\mathrm{VT},i}$, $i = 1 \ldots 4$. This algorithm can be seen as a lower bound for Channel-SLAM.
- **Alg. II**: Positioning algorithm using only the reflected and the LoS signal, assuming perfect knowledge of the geometry, hence, the knowledge of the states of VT_1. This reflects algorithms in [21], [22]. For $t_k > 10$, the algorithm uses only the reflected path for positioning.
- **Alg. III**: Positioning algorithm which considers the first arrived path as the LoS path. Hence, the algorithm interprets the second path (scattered path) as the LoS path for $t_k > 10$ and represents a multipath mitigation algorithm similar to [16].
- **Alg. IV**: Positioning algorithm using only the LoS path. For $t_k > 10$, the algorithm estimates the position using the movement prediction model. Therefore, the algorithm could be described as a multipath mitigation algorithm including an ideal NLoS detection.

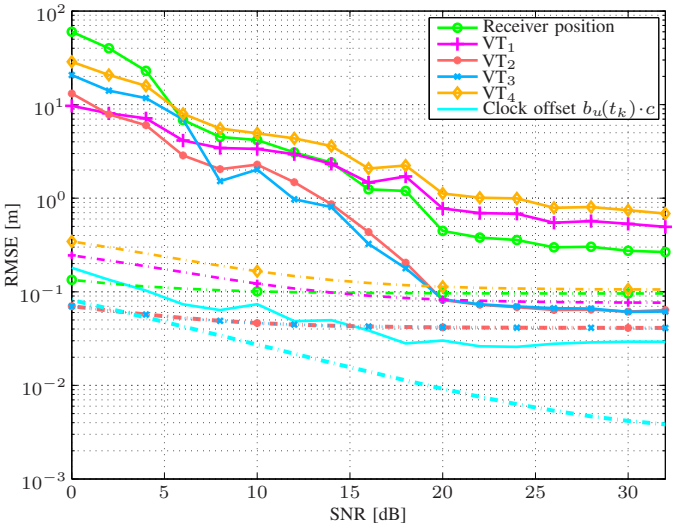

Fig. 4. RMSEs of the estimated receiver position, estimated VT positions and estimated clock offset versus SNR at the end of the track at $t_k = 20\,\mathrm{s}$ shown by the solid lines. The dashed lines represent the corresponding curves calculated by the PCRLBs.

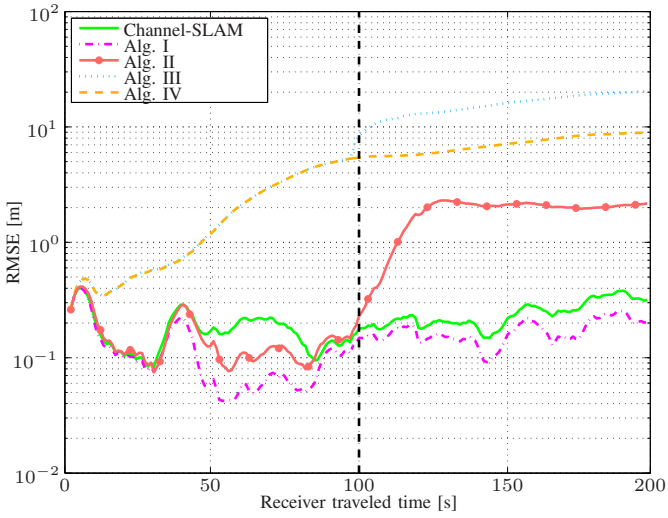

Fig. 5. RMSEs of the estimated receiver position versus receiver traveled time for different algorithms. The vertical dashed line indicates the time when the LoS component is lost.

Similarly to Channel-SLAM, these algorithms use the delays and AoAs of the estimated MPCs provided by KEST as input, use the same movement model, assume the knowledge of starting position and direction and are implemented using PFs with $N_s = 6000$ particles. Fig. 5 shows the RMSE versus the receiver traveled time for Channel-SLAM and Alg. I - IV. The vertical dashed line indicates the time when the LoS path is not received anymore. At the starting time, the RMSE for all algorithms are similar because of the same initialization. Alg. I can be interpreted as a lower bound and estimates the receiver position with the lowest RMSE. Alg. II shows similar results, as long as the LoS path prevails. When the LoS path is absent, the RMSE increases because the number

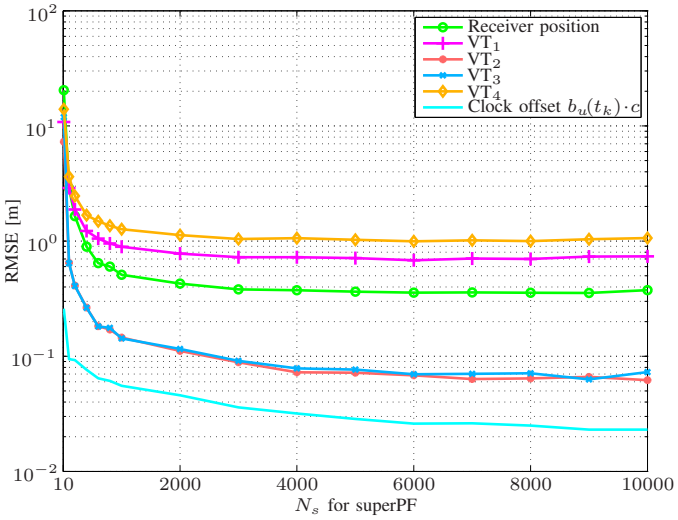

Fig. 6. RMSEs of the estimated receiver position, estimated VT positions and estimated clock offset versus number of particles at the end of the track at $t_k = 20\,\mathrm{s}$.

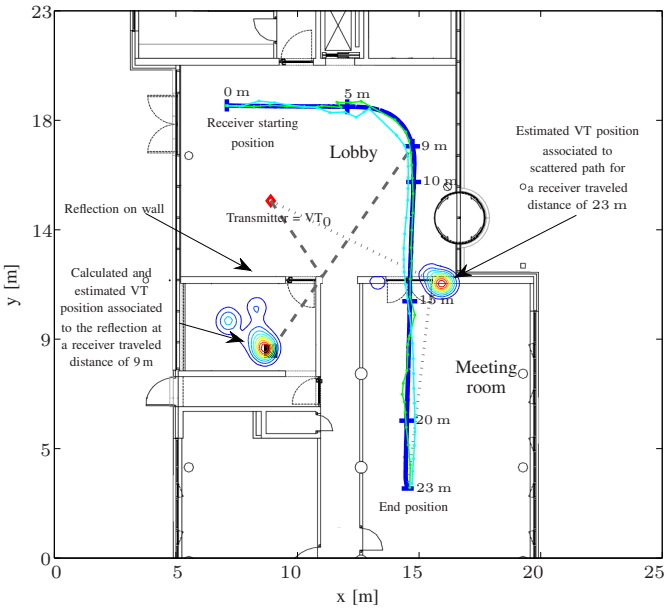

Fig. 7. Measurement scenario with a fixed transmitter and a moving receiver. The receiver is moving on the track as indicated in blue, starting in the lobby and entering after 14 m the meeting room. The green and cyan lines indicate the receiver position estimations of Channel-SLAM for two independent runs based on the same measurement data. Additionally, the PDFs of two estimated VT positions are shown, see also Fig. 8.

of transmitters reduces to one. Estimating the receiver position with only one path, like Alg. III and Alg. IV, the worst position accuracy is obtained compared to Alg. I, Alg. II and Channel-SLAM.

To evaluate the complexity of Channel-SLAM, Fig. 6 shows the RMSE for the receiver and VT positions at the end of the track, i.e. $t_k = 20\,\mathrm{s}$, versus different number of particles in the superPF. As mentioned before, the number of particles for the subPFs for each MPC with $i = 0, \ldots, 4$ is different depending on the estimated delay and AoA of each MPC. In average, the subPF uses for VT_1 $\mathbf{E}\left[N_{P,1,j}\right] = 2400$, for VT_2 $\mathbf{E}\left[N_{P,2,j}\right] = 2000$, for VT_3 $\mathbf{E}\left[N_{P,3,j}\right] = 3150$ and for VT_4 $\mathbf{E}\left[N_{P,4,j}\right] = 3700$ particles. The more particles for the superPF are used, the higher the accuracy of Channel-SLAM. However, with $N_s \geq 2000$, the receiver position can be estimated in average with an RMSE lower than $0.4\,\mathrm{m}$ within the simulated scenario.

B. Experimental Results

This section evaluates Channel-SLAM based on indoor channel measurements, indicated in Fig. 7 where we consider similarly to the simulations a LoS to NLoS transition. The measurement campaign was conducted using the MEDAV RUSK-DLR broadband channel sounder in single-input single-output (SISO) mode. The transmitter emitted a $1\,\mathrm{mW}$ multitone signal, see [50], with $N = 1281$ subcarriers with equal gains at a center frequency of $1.51\,\mathrm{GHz}$ with a bandwidth of $B = 100\,\mathrm{MHz}$. The CIR snapshots are repeatedly measured in a time grid of $T_g = 1.024\,\mathrm{ms}$. The transmit antenna was located in the lobby of the office building as visualized by the red diamond in Fig. 7, and the receive antenna was mounted on an experimental platform realized using a model train. The model train was running on a pre-measured track with a length of $23\,\mathrm{m}$ as indicated by the blue line in the office building, starting in the lobby and entering the meeting room after $14\,\mathrm{m}$ with a travel speed of $0.05\,\mathrm{m/s}$. To obtain the ground truth of the receiver for each captured CIR snapshot, the train is equipped with a rotary encoder which counts the number of motor turns. To measure the track location we used a tachymeter TPS1200 from Leica Geosystems AG which has an accuracy in subcentimeter domain based on distance and angular measurements. By knowing the traveled distance for each CIR snapshot, it is possible to form virtually a linear antenna array from the time-variant measurements, see also [51]. For these evaluations, we form a 3-element linear antenna array with an element-spacing of 0.3λ, where λ stands for the wavelength.

Fig. 8 shows the estimation results of KEST for the CIR versus the receiver traveled distance in meters. Only paths which are visible to the receiver for more than $5\,\mathrm{m}$ of movement are visualized. The vertical dashed line in Fig. 8 indicates the moment when the receiver is entering the meeting room (cf. Fig. 7). As shown in Fig. 8, many paths can be tracked for several meters of receiver movement. Channel-SLAM considers an underdetermined system, therefore, long visible paths are preferable. Thus for the evaluations, Channel-SLAM only uses these long tracked paths as visualized in Fig. 8. Anyhow, Channel-SLAM could use all detected MPCs, however, this would increase the computational complexity. The LoS path is visible to the receiver until the receiver enters the meeting room. Due to limited bandwidth and MPCs that are close to the LoS path, KEST is not able to resolve all paths properly. Hence, the KEST estimation of the LoS path length is not identical to the geometrical line-of-sight (GLoS) path length indicated by the black line in Fig. 8.

Similarly to the simulations in Section V-A, prior information of $\mathbf{x}_u(t_0)$ has been used. We apply a uniform distribution of $1\,\mathrm{m}$ width around the starting position $\boldsymbol{r}_u(t_0)$ and a uniform

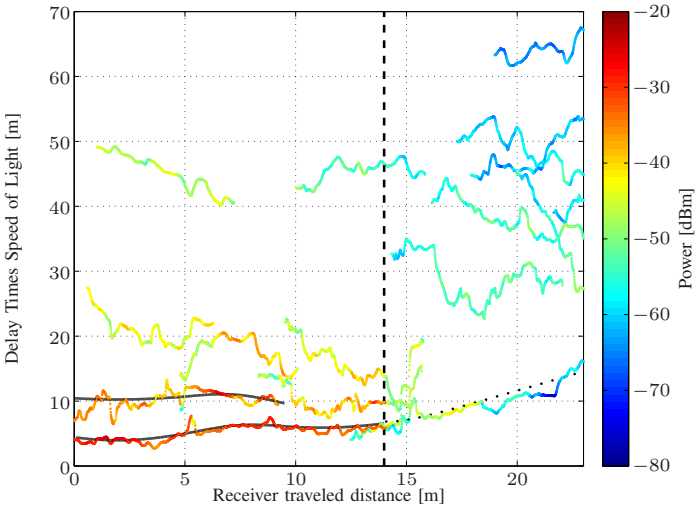

Fig. 8. Estimation results of KEST for the CIR versus the receiver traveled distance in meters. Only paths that are visible to the receiver for more than 5 m are shown. The vertical black dashed line indicates the traveled distance, when the mobile receiver enters the meeting room. The black solid line indicates the LoS path delay, the dashed line the calculated delay associated to a reflected path and the dotted line the calculated delay associated to the scattered path shown in Fig. 7.

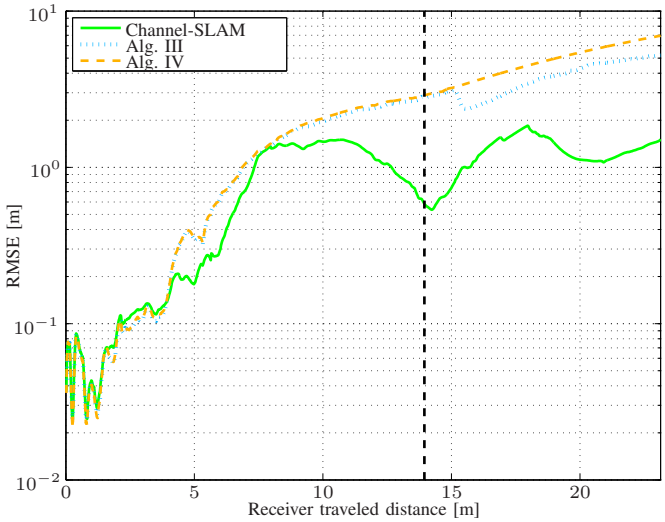

Fig. 9. $\mathrm{RMSE}_u(t_k)$ versus the receiver traveled distance for Channel-SLAM, Alg. III and Alg. IV, see Section V-A. The vertical black dashed line indicates the moment when the mobile receiver enters the meeting room.

distributed speed between $0\,\mathrm{m/s}$ and $0.2\,\mathrm{m/s}$ for $\|\boldsymbol{v}_u(t_0)\|$ while the speed direction is drawn from a uniform distribution of $60°$ width around the moving direction. For the evaluation, Channel-SLAM uses $N_s = 6000$ particles in the superPF. As mentioned before, for notational conveniences, the first MPC, i.e. $i = 0$, is considered as the LoS path to the physical transmitter and, therefore, the position $\boldsymbol{r}_{\mathrm{VT},0}(t_k) = \boldsymbol{r}_t$ is equal to the physical transmitter position and $d_{\mathrm{VT},0}(t_k) = 0$. Compared to the simulations in the previous section, the number of tracked MPCs changes, hence, the number of subPFs changes accordingly. The number of used MPCs and respectively the number of VTs changes between 2 at the starting point and up to 7 at the end of the track. In Fig. 7, we show by the green and cyan lines two examples of the MMSE point estimates of the receiver position for two different PF evaluations based on the same measurement data[4]. Additionally, Fig. 7 visualizes two VTs that might result from a reflected and scattered propagation path. On the left side of Fig. 7, the position of a VT occurring due to a reflection is displayed together with the estimated PDF from Channel-SLAM for a receiver travelled distance of 9 m. The estimated PDF of Channel-SLAM is indicated while the black square denotes the calculated VT position based on the hypothetical propagation path. A further comparison of the path to the hypothetical propagation is visualized in Fig. 8 comparing the delay estimate of KEST to the theoretical delay indicated by the dashed line. An additional VT is visualized in Fig. 7 on the right side as a PDF estimated by Channel-SLAM for a receiver traveled distance of 23 m. The VT is located at the edge of the entrance to the meeting room and corresponds, therefore, most probably to a scattered path which explains the rather low received power for the path. Again, the theoretical delay of the path is visualized in Fig. 8 as dotted line.

Please note, that because of the angular ambiguity by using a linear antenna array, two hypotheses of the VT position, on both sides of the linear antenna array are equally likely as long as the receiver moves along a straight line. Neither Channel-SLAM nor KEST can resolve the ambiguity. Hence, Channel-SLAM estimates the position of the VT on both sides of the antenna array that is aligned to the moving direction of the receiver. However, as long as the receiver moves on a straight track, both hypotheses do not influence the receiver position estimation results. By turning, the ambiguity can be solved, see also Section V-A. Therefore, for the considered reflected signal in Fig. 7 and Fig. 8, the ambiguity problem can be solved because the receiver turns at the receiver traveled distance between 5 m and 10 m. However, to overcome the ambiguity problem in general, a multidimensional antenna array able to estimate the two dimensional AoA could be used.

Because Channel-SLAM uses a PF, each evaluation result includes randomness. Therefore, we performed 200 independent evaluations using Channel-SLAM based on the same measurement data visualized by the estimated CIRs in Fig. 8. In Fig. 9, the green curve shows the average $\mathrm{RMSE}_u(t_k)$ for all evaluations and time instants. The vertical dashed line indicates the time instant when the LoS path is not received anymore. Because of the initialization of the receiver position using prior knowledge, the position error at the beginning of the track is rather low. Afterwards, the $\mathrm{RMSE}_u(t_k)$ is varying between 0.6 m and 1.1 m. Nevertheless, an average position accuracy below 1.1 m can be achieved within this indoor scenario. Similarly to Section V-A, Fig. 9 shows also the RMSE of Alg. III and Alg. IV. At the starting time, all algorithms perform similarly because of the same initialization.

[4]Please note, that the PF includes randomness, hence, even based on the same measurements, the MMSE estimates differ for each evaluation unless the number of particles is infinite.

$$\frac{\partial \boldsymbol{\mu}(\mathbf{x}(t_k))}{\partial \boldsymbol{r}_u(t_k)} = \sum_{i=0}^{N(t_k)-1} \left\{ \frac{j(2\pi f_c + \omega_m)\alpha_{i,l}(t_k) e^{-j(2\pi f_c+\omega_m)\tau_{i,l}(t_k)}}{c \cdot \| \boldsymbol{r}_{\mathrm{VT},i}(t_k) - (\boldsymbol{r}_u(t_k) + \frac{\boldsymbol{v}_u(t_k)\cdot(l-1)\cdot d}{\|\boldsymbol{v}_u(t_k)\|}) \|} \cdot \tilde{\mathbf{d}}_{\mathrm{VT},i,l}(t_k) \right\} \tag{39}$$

$$\frac{\partial \boldsymbol{\mu}(\mathbf{x}(t_k))}{\partial \boldsymbol{v}_u(t_k)} = \sum_{i=0}^{N(t_k)-1} \left\{ \frac{j \cdot (l-1) \cdot d \cdot (2\pi f_c + \omega_m)\alpha_{i,l}(t_k) e^{-j(2\pi f_c+\omega_m)\tau_{i,l}(t_k)}}{c \cdot \| \boldsymbol{r}_{\mathrm{VT},i}(t_k) - (\boldsymbol{r}_u(t_k) + \frac{\boldsymbol{v}_u(t_k)\cdot(l-1)\cdot d}{\|\boldsymbol{v}_u(t_k)\|}) \|} \times \left(\frac{\mathbf{I}}{\|\boldsymbol{v}_u(t_k)\|} - \frac{\boldsymbol{v}_u(t_k) \cdot \boldsymbol{v}_u(t_k)^T}{\|\boldsymbol{v}_u(t_k)\|^3} \right) \cdot \tilde{\mathbf{d}}_{\mathrm{VT},i,l}(t_k) \right\} \tag{40}$$

$$\frac{\partial \boldsymbol{\mu}(\mathbf{x}(t_k))}{\partial b_u(t_k)} = \sum_{i=0}^{N(t_k)-1} -j(2\pi f_c + \omega_m)\alpha_{i,l}(t_k) e^{-j(2\pi f_c+\omega_m)\tau_{i,l}(t_k)} \tag{41}$$

$$\frac{\partial \boldsymbol{\mu}(\mathbf{x}(t_k))}{\partial \boldsymbol{r}_{\mathrm{VT},i}(t_k)} = \frac{-j(2\pi f_c + \omega_m)\alpha_{i,l}(t_k) e^{-j(2\pi f_c+\omega_m)\tau_{i,l}(t_k)}}{c \cdot \| \boldsymbol{r}_{\mathrm{VT},i}(t_k) - (\boldsymbol{r}_u(t_k) + \frac{\boldsymbol{v}_u(t_k)\cdot(l-1)\cdot d}{\|\boldsymbol{v}_u(t_k)\|}) \|} \cdot \tilde{\mathbf{d}}_{\mathrm{VT},i,l}(t_k) \tag{42}$$

$$\frac{\partial \boldsymbol{\mu}(\mathbf{x}(t_k))}{\partial d_{\mathrm{VT},i}(t_k)} = -j(2\pi f_c + \omega_m)\alpha_{i,l}(t_k) e^{-j(2\pi f_c+\omega_m)\tau_{i,l}(t_k)} \frac{1}{c} \tag{43}$$

VI. Discussion on Practical Implementation

The paper focuses on Channel-SLAM, derives the algorithm and provides performance results. In order to use Channel-SLAM in potential applications, some aspects have to be considered which are briefly discussed in the following. Channel-SLAM relies on estimated and tracked CIRs at the receiver side, hence, it is essential that the transmitter emits continuously wideband reference signals and that the receiver is equipped with a linear antenna array. As mentioned in [36], instead of using a linear antenna array, the moving receiver could also be equipped with one antenna and a gyroscope to obtain heading information of the moving receiver. To use multipath propagation for positioning, Channel-SLAM relies on tracking the MPCs' parameters over the receiver movement as the number of measurements for a MPC is smaller than the number of parameters to be estimated at a certain time instant. Therefore, in a real-time algorithm, new MPCs should be first tracked for a certain time interval. After the MPCs have been tracked for some time, Channel-SLAM can re-estimate the receiver positions and the states of the VTs simultaneously based on these MPCs. Furthermore, Channel-SLAM is based on a ray optical model for MPCs such that dense MPCs need to be considered either on the lower level like in KEST or a model mismatch error might occur. Additionally, in the described evaluations, we assume the knowledge of the starting position, in order to fix the coordinate system. In general, Channel-SLAM works in a local coordinate system which may be transferred into a global coordinate system by using other sensors like GNSS. For simplicity, the derived algorithm does not consider clock drifts where appropriate models have to be used. Furthermore, Channel-SLAM assumes a static environment, hence, dynamic scatterers like in a car-to-car scenario are not included.

VII. Conclusion

This paper presents an algorithm for multipath assisted positioning named Channel-SLAM. The novel positioning method takes advantage of the multipath components instead of mitigating them. Compared to similar approaches, the proposed algorithm does not need prior information such as the room-layout or a database for fingerprinting except of the knowledge of the physical transmitter position as well as the initial receiver states that are position and speed. Channel-SLAM exploits paths occurring due to reflections, scattering and the combination of both phenomena. We demonstrate that each multipath component can be treated as emitted from a virtual transmitter with unknown but fixed position. Interpreting the virtual transmitters as landmarks allows to use a simultaneous localization and mapping (SLAM) methodology to estimate the landmarks and the receiver position jointly. Therefore, multipath components are treated as additional transmitters enabling to estimate the receiver position using only one physical transmitter. To verify the position accuracy of Channel-SLAM a comparison to the posterior Cramér-Rao lower bound and to four simplified algorithms is performed based on simulations. An accuracy below 0.3 m in the simulated scenario can be achieved using only one physical transmitter for signal-to-noise-ratios greater than 20 dB. Additionally, the paper presents the performance of Channel-SLAM based on measurements in an indoor scenario with only one physical transmitter, where an average position accuracy below 1.1 m can be achieved. Future work will be done towards pedestrian and robots navigation in GNSS-challenging scenarios like urban canyons or indoors such as shopping malls.

Appendix

The derivative of $\boldsymbol{\mu}(\mathbf{x}(t_k))$ with respect to the user position $\boldsymbol{r}_u(t_k)$ is (39), with respect to the user velocity $\boldsymbol{v}_u(t_k)$ is (40), with respect to the clock bias $b_u(t_k)$ is (41), with respect to the i-th virtual transmitter position $\boldsymbol{r}_{\mathrm{VT},i}(t_k)$ is (42), and with respect to the corresponding additional distance $d_{\mathrm{VT},i}(t_k)$ is (43).

REFERENCES

[1] G. Dedes and A. G. Dempster, "Indoor GPS Positioning - Challenges and Opportunities," in *Proc. IEEE Vehicular Technology Conf. Fall*, Sep. 2005, pp. 412–415.

[2] A. H. Sayed, A. Tarighat, and N. Khajehnouri, "Network-Based Wireless Location: Challenges Faced in Developing Techniques for Accurate Wireless Location Information," *IEEE Signal Process. Mag.*, vol. 22, pp. 24–40, Jul. 2005.

[3] Y. Zhao, "Standardization of Mobile Phone Positioning for 3G Systems," *IEEE Commun. Mag.*, vol. 40, no. 7, pp. 108–116, Jul. 2002.

[4] K. Kaemarungsi and P. Krishnamurthy, "Properties of Indoor Received Signal Strength for WLAN Location Fingerprinting," in *Proc. Int. Conf. on Mobile and Ubiquitous Systems: Computing, Networking and Services*, Aug. 2004, pp. 14–23.

[5] M. Win and R. Scholtz, "Characterization of Ultra-Wide Bandwidth Wireless Indoor Channels: a Communication-Theoretic View," *IEEE J. Sel. Areas Commun.*, vol. 20, no. 9, pp. 1613–1627, Dec. 2002.

[6] A. Molisch, D. Cassioli, C.-C. Chong, S. Emami, A. Fort, B. Kannan, J. Karedal, J. Kunisch, H. Schantz, K. Siwiak, and M. Win, "A Comprehensive Standardized Model for Ultrawideband Propagation Channels," *IEEE Trans. Antennas Propag.*, vol. 54, no. 11, pp. 3151–3166, Nov. 2006.

[7] C. Steiner and A. Wittneben, "Low Complexity Location Fingerprinting With Generalized UWB Energy Detection Receivers," *IEEE Trans. Signal Process.*, vol. 58, no. 3, pp. 1756–1767, Mar. 2010.

[8] B. W. Parkinson and J. J. Spilker Jr., *Global Positioning System: Theory and Applications, Vol. 1*. American Institute of Aeronautics and Astronautics Inc., 1996.

[9] A. J. van Dierendonck, P. Fenton, and T. Ford, "Performance Evaluation of the Multipath Estimating Delay Lock Loop," *Journal of the Institute of Navigation*, vol. 39, no. 3, pp. 265 – 284, Fall 1992.

[10] L. Garin, F. van Diggelen, and J.-M. Rousseau, "Strobe & Edge Correlator Multipath Mitigation for Code," in *Proc. 9th Int. Technical Meeting of the Satellite Division of The Institute of Navigation (ION GPS 1996)*, Kansas City, MO, USA, Sep. 1996.

[11] G. A. McGraw and M. S. Braasch, "GNSS Multipath Mitigation using Gated and High Resolution Correlator Concepts," in *Proc. National Technical Meeting of the Satellite Division of the Institute of Navigation*, San Diego, CA, USA, Jan. 1999.

[12] B. R. Townsend, P. C. Fenton, A. J. van Dierendonck, and D. J. R. V. Nee, "Performance Evaluation of the Multipath Estimating Delay Lock Loop," *Journal of the Institute of Navigation*, vol. 42, no. 3, pp. 503–514, Fall 1995.

[13] F. Antreich, J. Nossek, and W. Utschick, "Maximum Likelihood Delay Estimation in a Navigation Receiver for Aeronautical Applications," *Aerospace Science and Technology*, vol. 12, no. 3, pp. 256–267, Apr. 2008.

[14] B. H. Fleury, M. Tschudin, R. Heddergott, D. Dahlhaus, and K. I. Pedersen, "Channel Parameter Estimation in Mobile Radio Environments Using the SAGE Algorithm," *IEEE J. Sel. Areas Commun.*, vol. 17, no. 3, pp. 434–450, Mar. 1999.

[15] B. Krach, P. Robertson, and R. Weigel, "An Efficient Two-Fold marginalized Bayesian Filter for Multipath Estimation in Satellite Navigation Receivers," *EURASIP J. Adv. Sig. Proc.*, vol. 2010, Sep. 2010.

[16] P. Closas, C. Fernández-Prades, and J. A. Fernández-Rubio, "A Bayesian Approach to Multipath Mitigation in GNSS Receivers," *IEEE J. Sel. Areas Sig. Proc.*, vol. 3, no. 4, pp. 695–706, Aug. 2009.

[17] M. Triki, D. Slock, V. Rigal, and P. Francois, "Mobile Terminal Positioning via Power Delay Profile Fingerprinting: Reproducible Validation Simulations," in *Proc. IEEE Vehicular Technology Conf. Fall*, Sep. 2006, pp. 1–5.

[18] E. Kupershtein, M. Wax, and I. Cohen, "Single-Site Emitter Localization via Multipath Fingerprinting," *IEEE Trans. Signal Process.*, vol. 61, no. 1, pp. 10–21, Jan. 2013.

[19] Y. Shen and M. Win, "On the Use of Multipath Geometry for Wideband Cooperative Localization," in *Proc. IEEE Global Telecommunications Conf.*, Dec. 2009, pp. 1–6.

[20] M. Froehle, E. Leitinger, P. Meissner, and K. Witrisal, "Cooperative Multipath-Assisted Indoor Navigation and Tracking (Co-MINT) using UWB Signals," in *Proc. IEEE Int. Conf. on Communications*, Jun. 2013, pp. 16–21.

[21] E. Leitinger, P. Meissner, M. Lafer, and K. Witrisal, "Simultaneous Localization and Mapping using Multipath Channel Information," in *Proc. IEEE Int. Conf. on Communications*, June 2015, pp. 754–760.

[22] P. Meissner, K. Witrisal, and K.Witrisal, "UWB for Robust Indoor Tracking: Weighting of Multipath Components for Efficient Estimation," *IEEE Wireless Communications Letters*, vol. 3, no. 5, pp. 501–504, Oct. 2014.

[23] K. Witrisal and P. Meissner, "Performance bounds for multipath-assisted indoor navigation and tracking (MINT)," in *Proc. IEEE Int. Conf. on Communications*, Jun. 2012, pp. 4321–4325.

[24] Y. Kuang, K. Astrom, and F. Tufvesson, "Single Antenna Anchor-Free UWB Positioning based on Multipath Propagation," in *Proc. IEEE Int. Conf. on Communications*, Jun. 2013, pp. 5814–5818.

[25] M. Zhu, J. Vieira, Y. Kuang, K. Astrom, A. Molisch, and F. Tufvesson, "Tracking and Positioning using Phase Information from Estimated Multi-Path Components," in *Proc. IEEE Int. Conf. on Communications*, June 2015, pp. 712–717.

[26] T. Deissler and J. Thielecke, "Feature based Indoor Mapping using a Bat-Type UWB Radar," in *Proc. IEEE Int. Conf. Ultra-Wideband*, Sep. 2009, pp. 475–479.

[27] ——, "UWB SLAM with Rao-Blackwellized Monte Carlo Data Association," in *Proc. IEEE Int. Conf. on Indoor Positioning and Indoor Navigation*, Sep. 2010, pp. 1–5.

[28] R. Smith and P. Cheeseman, "On the Representation and Estimation of Spatial Uncertainty," *Int. J. Robotics Research*, vol. 5, no. 4, pp. 56–68, 1986.

[29] J. Leonard and H. Durrant-whyte, "Simultaneous Map Building and Localization For an Autonomous Mobile Robot," in *Proc. IEEE/RSJ Int. Workshop on Intelligent Robots and Systems*, Osaka , Japan, Nov. 1991.

[30] H. Durrant-Whyte and T. Bailey, "Simultaneous Localization and Mapping: Part I," *IEEE Robot. Autom. Mag.*, vol. 13, no. 2, pp. 99–110, Jun. 2006.

[31] V. La Tosa, B. Denis, and B. Uguen, "Joint Anchor-Less Tracking and Room Dimensions Estimation through IR-UWB Peer-to-Peer Communications," in *Proc. IEEE Int. Conf. Ultra-Wideband*, Sep. 2011, pp. 575–579.

[32] Y. Shen and M. Win, "Fundamental Limits of Wideband Localization: Part I: A General Framework," *Information Theory, IEEE Transactions on*, vol. 56, no. 10, pp. 4956–4980, 2010.

[33] C. Gentner and T. Jost, "Indoor Positioning using Time Difference of Arrival between Multipath Components," in *Proc. IEEE Int. Conf. on Indoor Positioning and Indoor Navigation*, Montbeliard, France, Oct. 2013.

[34] C. Gentner, T. Jost, and A. Dammann, "Accurate Indoor Positioning using Multipath Components," in *Proc. Int. Technical Meeting of the Satellite Division of the Institute of Navigation*, Nashville, TN, USA, Sep. 2013.

[35] C. Gentner, R. Pöhlmann, T. Jost, and A. Dammann, "Multipath Assisted Positioning using a Single Antenna with Angle of Arrival Estimations," in *Proc. Int. Technical Meeting of the Satellite Division of the Institute of Navigation*, Tampa, FL, USA, Sep. 2014.

[36] C. Gentner, R. Pöhlmann, M. Ulmschneider, T. Jost, and A. Dammann, "Multipath Assisted Positioning for Pedestrians," in *Proc. Int. Technical Meeting of the Satellite Division of the Institute of Navigation*, Tampa, FL, USA, Sep. 2015.

[37] A. Doucet, N. d. Freitas, K. P. Murphy, and S. J. Russell, "Rao-Blackwellised Particle Filtering for Dynamic Bayesian Networks," in *Proc. Conf. Uncertainty in Artificial Intelligence*, ser. UAI '00, 2000, pp. 176–183.

[38] G. L. Turin, "A Statistical Model of Urban Multipath Propagation," *IEEE Trans. Veh. Technol.*, vol. 21, no. 1, pp. 1–9, Feb. 1972.

[39] T. S. Rappaport, *Wireless Communications - Principles and Practice*. Prentice Hall, 1996.

[40] T. Jost, W. Wang, U.-C. Fiebig, and F. Pérez-Fontán, "Detection and Tracking of Mobile Propagation Channel Paths," *IEEE Trans. Antennas Propag.*, vol. 60, no. 10, pp. 4875–4883, Oct. 2012.

[41] J. Salmi, A. Richter, and V. Koivunen, "Detection and Tracking of MIMO Propagation Path Parameters Using State-Space Approach," *IEEE Trans. Signal Process.*, vol. 57, no. 4, pp. 1538–1550, Apr. 2009.

[42] M. Arulampalam, S. Maskell, N. Gordon, and T. Clapp, "A Tutorial on Particle Filters for Online Nonlinear/Non-Gaussian Bayesian Tracking," *IEEE Trans. Signal Process.*, vol. 50, no. 2, pp. 174–188, Feb. 2002.

[43] B. Ristic, S. Arulampalam, and N. Gordon, *Beyond the Kalman Filter: Particle Filters for Tracking Applications*. Artech House, 2004.

[44] M. Khider, S. Kaiser, and P. Robertson, "A Novel 3-Dimensional Movement Model for Pedestrian Navigation," *RIN Journal of Navigation*, vol. 65, no. 2, pp. 245–264, Mar. 2012.

[45] Y. Bar-Shalom, T. Kirubarajan, and X.-R. Li, *Estimation with Applications to Tracking and Navigation*. New York, NY, USA: John Wiley & Sons, Inc., 2002.
[46] M. Khider and T. Jost and P. Robertson and E. Abdo-Sánchez, "GNSS Pseudorange-Based Multisensor Positioning Incorporating a Multipath Error Model," *IET Radar, Sonar & Navigation*, vol. 7, no. 8, pp. 881–894, Oct. 2013.
[47] N. Gordon, D. Salmond, and A. F. M. Smith, "Novel Approach to Nonlinear/Non-Gaussian Bayesian State Estimation," *IEE Proc. Radar Signal Processing*, vol. 140, no. 2, pp. 107–113, 1993.
[48] P. Tichavsky, C. Muravchik, and A. Nehorai, "Posterior Cramér-Rao Bounds for Discrete-Time Nonlinear Filtering," *IEEE Trans. Signal Process.*, vol. 46, no. 5, pp. 1386–1396, May 1998.
[49] M. L. Hernandez, T. Kirubarajan, and Y. Bar-Shalom, "Multisensor Resource Deployment using Posterior Cramér-Rao Bounds," *IEEE Trans. Aerosp. Electron. Syst.*, vol. 40, no. 2, pp. 399–416, Apr. 2004.
[50] R. S. Thomä, M. Landmann, A. Richter, and U. Trautwein, *Smart Antennas - State of the Art*, ser. EURASIP Book Series on SP&C. Hindawi Publishing Corporation, 2005, pp. 241–270.
[51] W. Wang and T. Jost, "A Low-Cost Platform for Time-Variant Wireless Channel Measurements with Application to Positioning," *IEEE Trans. Instrum. Meas.*, vol. 61, no. 6, pp. 1597–1604, Jun. 2012.

Christian Gentner studied electrical engineering at the University of Applied Science in Ravensburg, with the main topic communication technology and received his Dipl.-Ing. (BA) degree in 2006. During this study he received practical experiences at Rohde & Schwarz in Munich. He continued his study at the University of Ulm until 2009, where he received his M.Sc. degree. He is currently working towards the Ph.D. degree at the Institute of Communications and Navigation of the German Aerospace Center (DLR). His current research focuses on multipath assisted positioning.

Thomas Jost (M'11) received a Diploma degree (FH) 2001 in Electrical Engineering from University of Applied Science Wiesbaden, Germany and a Diploma degree in 2003 in Electrical Engineering and Information Technology from Technical University of Darmstadt, Germany. In 2013, he received his PhD from University of Vigo, Spain. From 2003 to 2006 he held a research assistant position in the Signal Processing Group at TU Darmstadt. Since 2006 he is a member of the scientific staff of the Institute of Communications and Navigation at the German Aerospace Center.

Wei Wang (M'09) received the Bachelor degree in the field of communications engineering from University of Wuhan, China, in 2003, the Master degree from University of Kiel, Germany, in 2006 and the Doctoral degree from University of Erlangen-Nuremberg, Germany, in 2014. Since 2007, he works as a scientific staff member at the Institute of Communications and Navigation of German Aerospace Center (DLR), Oberpfaffenhofen, Germany. His research interests are channel characteristics analysis and modeling for localization/ navigation based on channel measurements, terrestrial radio based positioning/navigation and related topics.

Siwei Zhang received his M.Sc. degree in communication engineering in 2011 from the Technical University of Munich, Germany and his B.Sc. degree in electrical engineering in 2009 from Zhejiang University, China. Since 2012, he has been a scientific researcher at the German Aerospace Center (DLR). His research interests are in statistical signal processing, distributed systems, and radio-based navigation.

Armin Dammann received the Dipl.-Ing. (M.Sc.) and Dr.-Ing. (Ph.D.) degrees in Electrical Engineering from the University of Ulm, Germany, in 1997 and 2005 respectively. In 1997 he joined the Institute of Communications and Navigation of the German Aerospace Center (DLR). Since 2005 he is head of the Mobile Radio Transmission Research Group. His research interest and activities include signal design and signal processing for wireless communication and navigation systems. He has been active in several EU-projects, e.g., WINNER, WHERE and WHERE2.

Uwe-Carsten Fiebig was born in Augsburg, Germany, in 1962. He studied electrical engineering at the Technical University of Munich (TUM), Germany, and spent the last year of his studies at Ecole Supérieure en Electrotechnique et Electronique in Paris, France. In 1987 he received the Dipl.-Ing. degree from TUM and in 1993 the Dr.-Ing. degree from University of Kaiserslautern. Uwe-Carsten Fiebig joined the Institute of Communications and Navigation at DLR (German Aerospace Research), Oberpfaffenhofen, Germany, in 1988. In 1995 and 1996 he was guest scientist at the Communications Research Center, Ottawa, Canada, and at the Yokohama National University, Japan, respectively. Since 1994 Uwe-Carsten Fiebig is Head of the Department Communications Systems which carries out research in aeronautical and vehicular communications, multisensor navigation and swarm exploration. His current research interests include propagation and broadband channel modelling for satellite, aeronautical and vehicular environments. Uwe-Carsten Fiebig is honorary professor at the University of Ulm, Germany, and teaches satellite communications and navigation.